

RESEARCH PAPER



Design and synthesis of novel quinazolinone-based derivatives as EGFR inhibitors with antitumor activity

Amr Sonousi^a, Rasha A. Hassan^a, Eman O. Osman^a, Amr M. Abdou^b and Soha H. Emam^a

^aPharmaceutical Organic Chemistry Department, Faculty of Pharmacy, Cairo University, Cairo, Egypt; ^bDepartment of Microbiology and Immunology, National Research Centre, Dokki, Giza, Egypt

ABSTRACT

Nineteen new quinazolin-4(3*H*)-one derivatives **3a–g** and **6a–l** were designed and synthesised to inhibit EGFR. The antiproliferative activity of the synthesised compounds was tested *in vitro* against 60 different human cell lines. The most potent compound **6d** displayed superior sub-micromolar antiproliferative activity towards NSC lung cancer cell line NCI-H460 with $GI_{50} = 0.789 \mu\text{M}$. It also showed potent cytostatic activity against 40 different cancer cell lines (TGI range: 2.59–9.55 μM). Compound **6d** potently inhibited EGFR with $IC_{50} = 0.069 \pm 0.004 \mu\text{M}$ in comparison to erlotinib with IC_{50} value of $0.045 \pm 0.003 \mu\text{M}$. Compound **6d** showed 16.74-fold increase in total apoptosis and caused cell cycle arrest at G1/S phase in breast cancer HS 578T cell line. Moreover, the most potent derivatives were docked into the EGFR active site to determine their binding mode and confirm their ability to satisfy the pharmacophoric features required for EGFR inhibition.

ARTICLE HISTORY

Received 27 June 2022
Revised 23 August 2022
Accepted 24 August 2022

KEYWORDS

Quinazolin-4(3*H*)-one; antiproliferative activity; molecular modelling; EGFR inhibition; cell cycle analysis

Introduction



Cancer is a widespread and lethal noncommunicable disease with rapidly growing incidence and mortality worldwide¹. Breast cancer is the leading cause of death among women with a reported incidence of approximately 2.3 million and 685,000 deaths worldwide in 2020².


Molecular targeting therapy approach, that targets a crucial cancer-related enzyme or receptor, increases the tumour specificity and decreases the side effects^{3–5}. The epidermal growth factor receptor (EGFR) is mainly involved in the growth factor signalling. Abnormal signalling and overexpression of this receptor enhance downstream effects such as cell survival, cell proliferation and angiogenesis which lead to uncontrolled cell proliferation and metastasis, which ultimately promote tumour growth (Figure 1)⁶. The EGFR is one of the members of ErbB tyrosine kinase receptors family⁷, and consists of two domains; an extracellular receptor domain connected via a transmembrane region to an intracellular domain with tyrosine kinase function⁸. Inhibition of EGFR by tyrosine kinase inhibitors (TKIs) delays these downstream effects and lead to inhibition of tumour growth. Many breast cancers express 2×10^6 EGFR molecules per cell which is more than 20-fold the expression of EGFR in normal cells^{9,10}. This overexpression of EGFR in breast cancer as well as other cancer cells including colon and lung cancers made this a potential molecular target for inhibition^{11–14}.

Three generations of small-molecule EGFR TKIs have been developed so far^{15,16}. The first-generation, such as gefitinib and erlotinib usually with 4-anilinoquinazoline motifs, achieves initial good responses in the treatment of cancer patients with

overexpression of EGFR but unfortunately, resistance to this class was acquired by most patients within 1 year¹⁷. The second-generation of EGFR TKIs, such as neratinib and afatinib, were developed to overcome the acquired resistance^{18,19}, however their associated side effects^{20,21} lead to the design of a novel class of third-generation EGFR TKIs, including osimertinib, rociletinib and olmutinib. This class has been designed and developed to overcome resistance and reduce side effects²². The aim of this study is to design, synthesise and evaluate compounds with the same pharmacophoric features as the third generation EGFR TKIs.

In previous studies in our lab, we synthesised different TKIs with high therapeutic index^{23–27}. In the present study, the design of the new compounds started by finding common pharmacophoric structural features of the newer generations of EGFR TKI without including the acrylamide moiety. The acrylamide moiety in the second and the third generations gives strong covalent binding to the SH group in Cys797 residue of the receptor. However, these compounds are prone to drug resistance when this irreversible covalent interaction is lost due to C797S mutation^{28,29}. The common structural features were found to be (A) an upper aryl ring attached to (B) 2-aminopyrimidines or 2-amino arylfusedpyrimidines and the 2-amino is attached to either C) phenoxy group or piperazinyl aryl group (Figure 2). The design of the novel compounds was done to mimic these structural features of the third generation EGFR TKIs to have 2-aminoarylquinazoline linked to an upper aryl ring and the 2-amino is attached to either substituted phenoxy group (**3a–d**) or piperazinyl aryl (or its isostere) (**3e–g**). We also designed congener compounds with a 2-thioacetyl spacer between the pyrimidine ring and either phenoxy group (**6a–f**) or piperazinyl aryl (**6g–l**) groups to investigate

CONTACT Amr Sonousi  amr.motawi@pharma.cu.edu.eg  Department of Pharmaceutical Organic Chemistry, Faculty of Pharmacy, Cairo University, 33 Kasr El-Aini Street, Cairo, 11562, Egypt.

 Supplemental data for this article can be accessed online at <https://doi.org/10.1080/14756366.2022.2118735>.

© 2022 The Author(s). Published by Informa UK Limited, trading as Taylor & Francis Group.

This is an Open Access article distributed under the terms of the Creative Commons Attribution License (<http://creativecommons.org/licenses/by/4.0/>), which permits unrestricted use, distribution, and reproduction in any medium, provided the original work is properly cited.

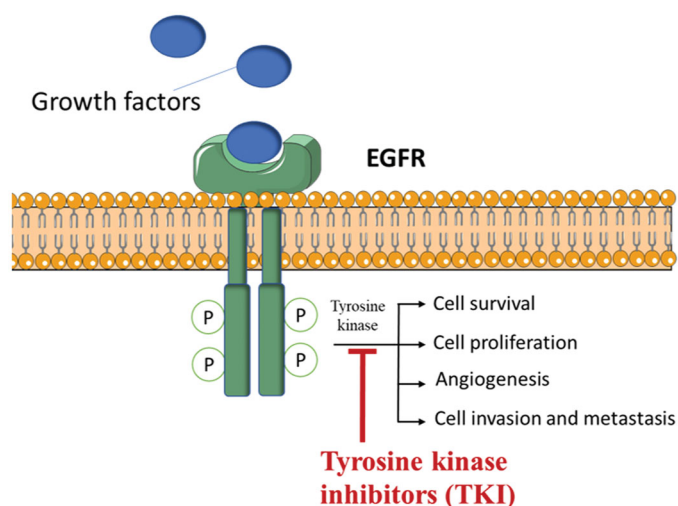


Figure 1. An illustrative diagram showing the mechanism of action of TKIs as anticancer.

the effect of this spacer on the activity of the compounds (Figure 2). The designed compounds were synthesised and subjected to *in vitro* screening of their cytotoxic activity against a panel of 60 different cancer cell lines. The compounds were investigated for their ability to inhibit EGFR, their effect on cancer cell cycle and their ability to induce apoptosis. Molecular modelling studies were done as well to rationalise the biological activity of the synthesised compounds.

Experimental

Chemistry

General

Melting points were obtained on a Griffin apparatus and were uncorrected. Microanalyses for C, H and N were carried out at the Regional Centre for Mycology and Biotechnology, Faculty of Pharmacy, Al-Azhar University. IR spectra were recorded on Shimadzu IR 435 spectrophotometer (Shimadzu Corp., Kyoto, Japan) Faculty of Pharmacy, Cairo University, Cairo, Egypt, and values were represented in cm^{-1} . ^1H NMR spectra were carried out on Bruker 400 MHz (Bruker Corp., Billerica, MA, USA) spectrophotometer, Faculty of Pharmacy, Cairo University, Cairo, Egypt. The chemical shifts were recorded in ppm on δ scale, coupling constants (J) were given in Hz and peak multiplicities are designed as follows: s, singlet; d, doublet; dd, doublet of doublets; t, triplet; m, multiplet. ^{13}C NMR spectra were carried out on Bruker 100 MHz spectrophotometer, Faculty of Pharmacy, Cairo University, Cairo, Egypt. Mass spectra were recorded with Advion expression[®] CMS, Nawah Scientific, Cairo, Egypt. Progress of the reactions were monitored by TLC using precoated aluminium sheet silica gel MERCK 60 F 254 and was visualised by UV lamp. The original NMR spectra of the investigated compounds are provided as supporting information. Compounds **1a,b**^{30,31}, **2a,b**³¹, **4a,b**^{32,33} and **5a,b**^{32,33} were prepared as reported.

General procedure for the preparation of 2-(2-(4-(4-substituted)benzylidene)hydrazinyl)-3-phenylquinazolin-4(3H)-one (3a-g). To a mixture of 2-hydrazino-quinazolinone **2a,b** (5 mmol) and the appropriate aryloxybenzaldehydes or dialkylaminobenzaldehydes (5 mmol) in absolute ethanol (50 mL), few drops of acetic acid

were added, and the reaction mixture was refluxed for 6 h then cooled. The precipitate, formed upon cooling, was collected by filtration, washed with water crystallised from ethanol to give the corresponding hydrazone derivative **3a-g**.

2-(2-(4-(4-chlorophenoxy)benzylidene)hydrazinyl)-3-phenylquinazolin-4(3H)-one (3a). Yellow solid: 89% yield; mp 158–164 °C; IR (KBr, cm^{-1}) 3444 (NH), 3078 (CH aromatic), 2924, 2854 (CH aliphatic), 1651 (C=O), 1593 (C=N); ^1H NMR (400 MHz, DMSO- d_6) δ 10.58 (NH, D₂O exchangeable), 8.06 (s, 1H, CH=N), 7.96 (d, $J=8.8$ Hz, 2H, ArH), 7.91 (d, $J=7.2$ Hz, 1H, ArH), 7.69–7.66 (m, 2H, ArH), 7.52–7.41 (m, 5H, ArH), 7.35–7.32 (m, 2H, ArH), 7.19–7.15 (m, 1H, ArH), 7.10–7.05 (m, 4H, ArH); ^{13}C NMR (100 MHz, DMSO- d_6) δ 161.1, 158.0, 155.6, 152.8, 151.8, 140.4, 136.9, 135.5, 131.4, 130.4, 130.2, 129.7, 129.3, 128.4, 128.0, 127.8, 122.3, 121.0, 118.9, 116.1, 114.8; Anal. Calcd for C₂₇H₁₉ClN₄O₂: C, 69.45; H, 4.10; N, 12.00; found C, 69.19; H, 4.28; N, 12.26; MS (ESI) m/z : 465 [M – H][–].

2-(2-(4-(4-bromophenoxy)benzylidene)hydrazinyl)-3-phenylquinazolin-4(3H)-one (3b). White solid: 92% yield; mp 198–200 °C; IR (KBr, cm^{-1}) 3332 (NH), 3051 (CH aromatic), 2974, 2943 (CH aliphatic), 1685 (C=O), 1616 (C=N); ^1H NMR (400 MHz, DMSO- d_6) δ 10.59 (NH, D₂O exchangeable), 8.06 (s, 1H, CH=N), 7.96 (d, $J=8.4$ Hz, 2H, ArH), 7.91 (d, $J=7.6$ Hz, 1H, ArH), 7.71–7.66 (m, 2H, ArH), 7.57 (d, $J=8.4$ Hz, 2H, ArH), 7.50 (t, $J=7.6$ Hz, 2H, ArH), 7.41–7.40 (m, 1H, ArH), 7.34 (d, $J=7.6$ Hz, 2H, ArH), 7.18–7.14 (m, 1H, ArH), 7.07 (d, $J=8.0$ Hz, 2H, ArH), 7.03 (d, $J=8.0$ Hz, 2H, ArH); ^{13}C NMR (100 MHz, DMSO- d_6) δ 161.1, 157.8, 156.1, 152.8, 151.8, 140.3, 136.9, 135.6, 133.4, 131.4, 130.2, 129.7, 129.3, 128.4, 127.8, 122.3, 121.4, 119.0, 116.1, 115.9, 114.8.; Anal. Calcd for C₂₇H₁₉BrN₄O₂: C, 63.42; H, 3.75; N, 10.96, found C, 63.19; H, 3.87; N, 11.20.

2-(2-(4-(4-methoxyphenoxy)benzylidene)hydrazinyl)-3-phenylquinazolin-4(3H)-one (3c). Yellow solid: 80% yield; mp 185–188 °C; IR (KBr, cm^{-1}) 3332 (NH), 3094 (CH aromatic), 2962, 2846 (CH aliphatic), 1681 (C=O), 1600 (C=N); ^1H NMR (400 MHz, DMSO- d_6) δ 10.57 (NH, D₂O exchangeable), 8.03 (s, 1H, CH=N), 7.92–7.89 (m, 3H, ArH), 7.69–7.66 (m, 2H, ArH), 7.51–7.47 (m, 2H, ArH), 7.44–7.39 (m, 1H, ArH), 7.35–7.32 (m, 2H, ArH), 7.18–7.14 (m, 1H, ArH), 7.06–7.03 (m, 2H, ArH), 7.01–6.97 (m, 2H, ArH), 6.97–6.93 (m, 2H, ArH), 3.76 (s, 3H, OCH₃); ^{13}C NMR (100 MHz, DMSO- d_6) δ 161.1, 159.8, 156.4, 153.0, 151.6, 149.2, 140.4, 136.9, 135.5, 130.2, 130.0, 129.7, 129.3, 128.4, 127.8, 122.2, 121.5, 117.3, 116.1, 115.6, 114.8, 55.9; Anal. Calcd for C₂₈H₂₂N₄O₃: C, 72.71; H, 4.79; N, 12.11; found C, 72.53; H, 4.91; N, 12.38; MS (ESI) m/z : 463 [M + H]⁺.

2-(2-(4-(4-chlorophenoxy)benzylidene)hydrazinyl)-3-(4-chlorophenyl)quinazolin-4(3H)-one (3d). White solid: 85% yield; mp 212–214 °C; IR (KBr, cm^{-1}) 3340 (NH), 3059 (CH aromatic), 2958, 2924 (CH aliphatic), 1693 (C=O), 1612 (C=N); ^1H NMR (400 MHz, DMSO- d_6) δ 10.61 (NH, D₂O exchangeable), 8.09 (s, 1H, CH=N), 7.96 (d, $J=8.4$ Hz, 2H, ArH), 7.91 (d, $J=7.6$ Hz, 1H, ArH), 7.70–7.66 (m, 2H, ArH), 7.57–7.54 (m, 2H, ArH), 7.48–7.44 (m, 2H, ArH), 7.42–7.39 (m, 2H, ArH), 7.19–7.15 (m, 1H, ArH), 7.10–7.06 (m, 4H, ArH); ^{13}C NMR (100 MHz, DMSO- d_6) δ 161.0, 158.0, 155.6, 153.0, 151.7, 140.4, 135.8, 135.6, 133.0, 131.7, 131.4, 130.4, 130.2, 129.4, 128.0, 127.8, 122.3, 121.0, 118.9, 116.1, 114.7; Anal. Calcd for C₂₇H₁₈Cl₂N₄O₂: C, 64.68; H, 3.62; N, 11.17, found C, 64.90; H, 3.85; N, 11.39.

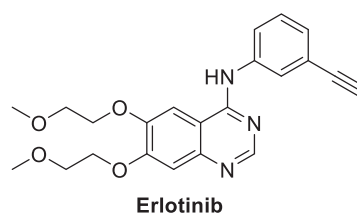
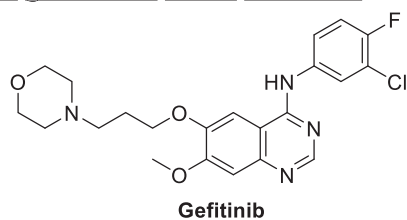
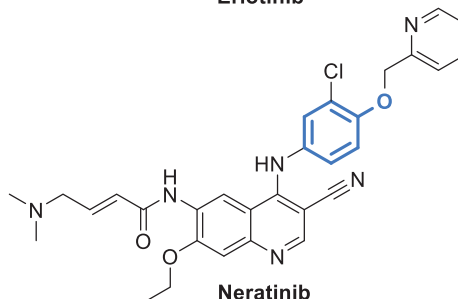
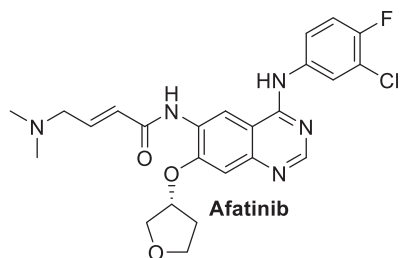
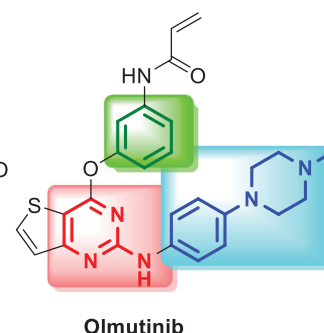
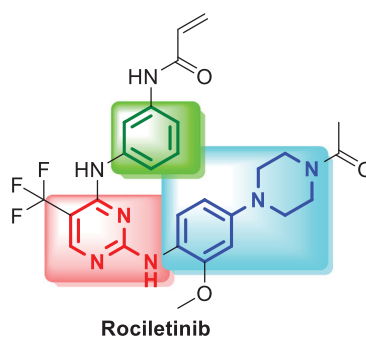
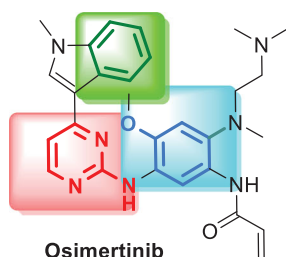
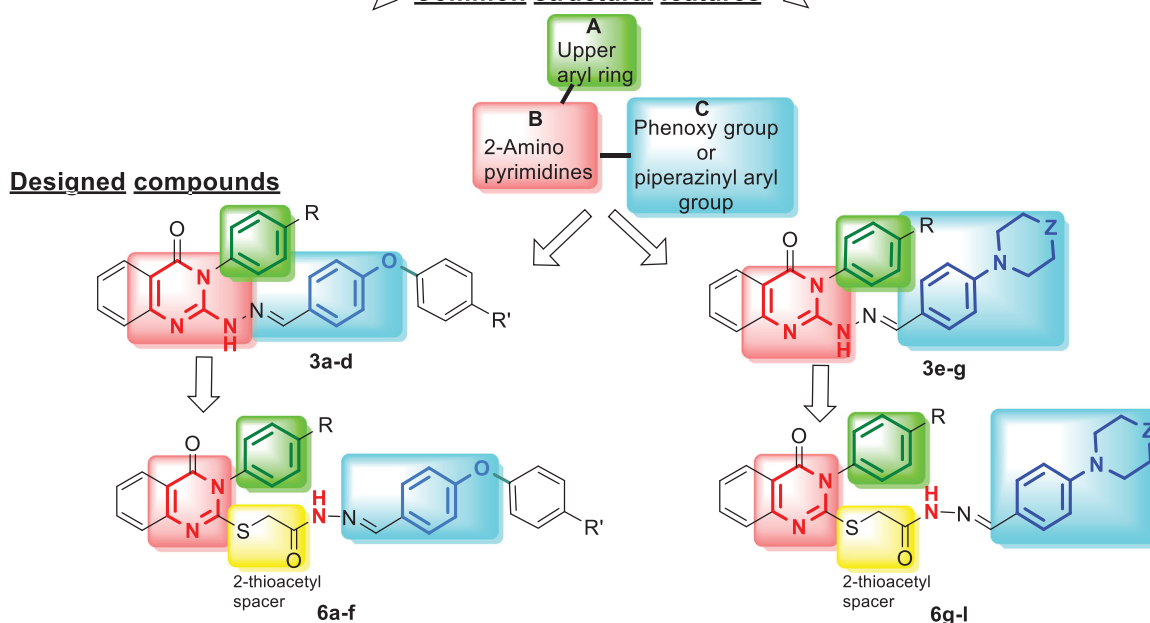
First generation EGFR inhibitors**Second generation EGFR inhibitors****Third generation EGFR inhibitors****Common structural features**

Figure 2. The three generations of EGFR inhibitors and the designed target compounds.

3-phenyl-2-(2-(4-(piperidin-1-yl)benzylidene)hydrazinyl)quinazolin-4(3H)-one (3e). Pale yellow solid: 82% yield; mp 160–166 °C; IR (KBr, cm^{-1}) 3332 (NH), 3051 (CH aromatic), 2924, 2846 (CH aliphatic), 1681 (C=O), 1600 (C=N); ^1H NMR (400 MHz, DMSO-d_6) δ

10.49 (NH, D_2O exchangeable), 7.93 (s, 1H, CH=N), 7.90 (d, $J=7.6$ Hz, 1H, ArH), 7.73 (d, $J=8.4$ Hz, 2H, ArH), 7.67 (d, $J=3.6$ Hz, 2H, ArH), 7.51–7.47 (m, 2H, ArH), 7.43–7.40 (m, 1H, ArH), 7.34–7.32 (m, 2H, ArH), 7.16–7.12 (m, 1H, ArH), 6.92 (d, $J=8.8$ Hz, 2H, ArH),

3.24 (t, $J=4.4$ Hz, 4H, 2CH₂ piperidine), 1.62–1.53 (m, 6H, 3CH₂ piperidine); ¹³C NMR (100 MHz, DMSO-d₆) δ 161.1, 154.0, 152.7, 150.8, 140.5, 137.0, 135.5, 129.7, 129.6, 129.3, 128.3, 127.8, 125.1, 122.0, 116.0, 114.9, 114.7, 49.0, 25.5, 24.4; Anal. Calcd for C₂₆H₂₅N₅O: C, 73.74; H, 5.95; N, 16.54, found C, 73.79; H, 5.80; N, 16.41; MS (ESI) m/z : 446 [M + Na⁺].

2-(2-(4-morpholinobenzylidene)hydrazinyl)-3-phenylquinazolin-4(3H)-one (3f). White solid: 79% yield; mp 242–244 °C; IR (KBr, cm⁻¹) 3325 (NH), 3092 (CH aromatic), 2939, 2894 (CH aliphatic), 1680 (C=O), 1604 (C=N); ¹H NMR (400 MHz, DMSO-d₆) δ 10.50 (NH, D₂O exchangeable), 7.94 (s, 1H, CH=N), 7.90 (d, $J=7.6$ Hz, 1H, ArH), 7.77 (d, $J=8.4$ Hz, 2H, ArH), 7.67 (d, $J=4.0$ Hz, 2H, ArH), 7.51–7.47 (m, 2H, ArH), 7.43–7.39 (m, 1H, ArH), 7.34–7.31 (m, 2H, ArH), 7.16–7.12 (m, 1H, ArH), 6.96 (d, $J=8.8$ Hz, 2H, ArH), 3.74 (t, $J=4.6$ Hz, 4H, 2CH₂ morpholine), 3.19 (t, $J=4.6$ Hz, 4H, 2CH₂ morpholine); ¹³C NMR (100 MHz, DMSO-d₆) δ 161.2, 153.9, 152.4, 151.0, 140.4, 136.8, 135.6, 129.6, 129.5, 129.4, 128.4, 127.8, 126.0, 122.1, 116.0, 114.6, 66.4, 48.0; Anal. Calcd for C₂₅H₂₃N₅O₂: C, 70.57; H, 5.45; N, 16.46; found C, 70.78; H, 5.71; N, 16.70; MS (ESI) m/z : 448 [M + Na⁺].

2-(2-(4-(4-methylpiperazin-1-yl)benzylidene)hydrazinyl)-3-phenylquinazolin-4(3H)-one (3g). Yellow solid: 85% yield; mp 208–210 °C; IR (KBr, cm⁻¹) 3325 (NH), 3093 (CH aromatic), 2974, 2890 (CH aliphatic), 1678 (C=O), 1612 (C=N); ¹H NMR (400 MHz, DMSO-d₆) δ 10.50 (NH, D₂O exchangeable), 7.93 (s, 1H, CH=N), 7.89 (d, $J=8.0$ Hz, 1H, ArH), 7.75 (d, $J=8.0$ Hz, 2H, ArH), 7.66 (d, $J=4.0$ Hz, 2H, ArH), 7.51–7.47 (m, 2H, ArH), 7.43–7.39 (m, 1H, ArH), 7.34–7.31 (m, 2H, ArH), 7.16–7.12 (m, 1H, ArH), 6.96–6.93 (m, 2H, ArH), 3.22 (t, $J=4.8$ Hz, 4H, 2CH₂ piperazine), 2.44 (t, $J=4.8$ Hz, 4H, 2CH₂ piperazine), 2.22 (s, 3H, NCH₃); ¹³C NMR (100 MHz, DMSO-d₆) δ 161.1, 153.9, 152.3, 150.9, 140.5, 136.9, 135.5, 129.7, 129.7, 129.5, 129.3, 128.3, 127.8, 125.7, 122.0, 116.0, 114.8, 114.7, 112.0, 54.9, 47.7, 46.2; Anal. Calcd for C₂₆H₂₆N₆O: C, 71.21; H, 5.98; N, 19.16, found C, 71.37; H, 6.12; N, 19.04; MS (ESI) m/z : 461 [M + Na⁺].

General procedure for the preparation of N'-(4-(4-substituted)benzylidene)-2-((4-oxo-3-aryl-3,4-dihydroquinazolin-2-yl)thio)acetohydrazide derivatives (6a-l). To a mixture of acetohydrazide derivatives **5a,b** (5 mmol) and the appropriate aryloxybenzaldehydes or dialkylaminobenzaldehydes (5 mmol) in ethanol (50 mL), few drops of acetic acid were added, and the reaction mixture was refluxed for 6 h then cooled. The precipitate was filtered, washed with water crystallised from ethanol to give the corresponding acetohydrazide derivatives **6a-l**.

N'-(4-(4-chlorophenoxy)benzylidene)-2-((4-oxo-3-phenyl-3,4-dihydroquinazolin-2-yl)thio)acetohydrazide (6a). White solid: 88% yield; mp 204–206 °C; IR (KBr, cm⁻¹) 3448, 3194 (OH/NH), 3066 (CH aromatic), 2970, 2943 (CH aliphatic), 1681 (C=O), 1608 (C=N); ¹H NMR (400 MHz, DMSO-d₆) δ 11.73, 11.61 (2s, 1H, OH/NH, D₂O exchangeable), 8.24, 8.04 (2s, 1H, CH=N), 8.10–8.07 (m, 1H, ArH), 7.86–7.77 (m, 1H, ArH), 7.73–7.70 (m, 2H, ArH), 7.61–7.58 (m, 3H, ArH), 7.51–7.44 (m, 6H, ArH), 7.11–7.04 (m, 4H, ArH), 4.46, 3.99 (2s, 2H, CH₂C=O); ¹³C NMR (100 MHz, DMSO-d₆) δ 169.1, 163.9, 161.1, 161.1, 158.5, 158.3, 157.4, 157.2, 155.3, 155.2, 147.6, 146.5, 143.1, 136.3, 136.2, 135.4, 130.5, 130.4, 130.0, 130.0, 129.9, 129.5, 129.2, 128.4, 128.3, 127.1, 126.5, 121.5, 121.3, 120.0, 120.0, 119.1, 118.9, 35.9, 34.7; Anal. Calcd for C₂₉H₂₁ClN₄O₃S: C, 64.38; H, 3.91; N,

10.36, found C, 64.51; H, 4.17; N, 10.62; MS (ESI) m/z : 563 [M + Na⁺].

N'-(4-(4-bromophenoxy)benzylidene)-2-((4-oxo-3-phenyl-3,4-dihydroquinazolin-2-yl)thio)acetohydrazide (6b). White solid: 82% yield; mp 224–226 °C; IR (KBr, cm⁻¹) 3444, 3182 (OH/NH), 3074 (CH aromatic), 2954, 2912 (CH aliphatic), 1681 (C=O), 1608 (C=N); ¹H NMR (400 MHz, DMSO-d₆) δ 11.73, 11.61 (2s, 1H, OH/NH, D₂O exchangeable), 8.24, 8.04 (2s, 1H, CH=N), 8.10–8.06 (m, 1H, ArH), 7.86–7.77 (m, 1H, ArH), 7.73–7.70 (m, 2H, ArH), 7.64–7.55 (m, 5H, ArH), 7.51–7.44 (m, 4H, ArH), 7.08–7.03 (m, 4H, ArH), 4.46, 3.99 (2s, 2H, CH₂C=O); ¹³C NMR (100 MHz, DMSO-d₆) δ 169.2, 164.1, 161.2, 161.1, 158.4, 158.1, 157.4, 157.2, 155.8, 155.7, 147.5, 147.5, 146.5, 143.2, 136.2, 136.1, 135.4, 133.4, 130.5, 130.5, 130.1, 130.0, 130.0, 129.8, 129.5, 129.2, 127.1, 126.6, 126.5, 126.4, 121.9, 121.7, 119.9, 119.9, 119.2, 119.0, 116.3, 116.2, 35.8, 34.6; Anal. Calcd for C₂₉H₂₁BrN₄O₃S: C, 59.49; H, 3.62; N, 9.57, found C, 59.70; H, 3.85; N, 9.70; MS (ESI) m/z : 583 [M - H]⁻ and 585 [M + 2 - H]⁻.

N'-(4-(4-methoxyphenoxy)benzylidene)-2-((4-oxo-3-phenyl-3,4-dihydroquinazolin-2-yl)thio)acetohydrazide (6c). Pale yellow solid: 83% yield; mp 128–130 °C; IR (KBr, cm⁻¹) 3441, 3182 (OH/NH), 3070 (CH aromatic), 2947, 2912 (CH aliphatic), 1681 (C=O), 1604 (C=N); ¹H NMR (400 MHz, DMSO-d₆) δ 11.68, 11.57 (2s, 1H, OH/NH, D₂O exchangeable), 8.21, 8.01 (2s, 1H, CH=N), 8.09–8.07 (m, 1H, ArH), 7.86–7.77 (m, 1H, ArH), 7.67–7.64 (m, 2H, ArH), 7.61–7.55 (m, 3H, ArH), 7.51–7.44 (m, 4H, ArH), 7.07–7.04 (m, 2H, ArH), 7.02–6.98 (m, 2H, ArH), 6.94 (t, $J=8.8$ Hz, 2H, ArH), 4.45, 3.99 (2s, 2H, CH₂C=O), 3.77, 3.76 (2s, 3H, OCH₃); ¹³C NMR (100 MHz, DMSO-d₆) δ 169.1, 163.8, 161.1, 160.3, 160.0, 157.4, 157.2, 156.5, 149.0, 148.9, 147.6, 146.7, 143.3, 136.3, 136.2, 135.4, 130.5, 130.4, 130.0, 129.9, 129.4, 129.1, 128.9, 127.1, 126.5, 121.8, 121.7, 120.0, 120.0, 117.6, 117.5, 115.7, 55.9, 35.9, 34.7; Anal. Calcd for C₃₀H₂₄N₄O₄S: C, 67.15; H, 4.51; N, 10.44, found C, 67.38; H, 4.72; N, 10.62; MS (ESI) m/z : 559 [M + Na⁺].

N'-(4-(4-chlorophenoxy)benzylidene)-2-((3-(4-chlorophenyl)-4-oxo-3,4-dihydroquinazolin-2-yl)thio)acetohydrazide (6d). White solid: 90% yield; mp 212–214 °C; IR (KBr, cm⁻¹) 3433, 3178 (OH/NH), 3089 (CH aromatic), 2978, 2947 (CH aliphatic), 1678 (C=O), 1608 (C=N); ¹H NMR (400 MHz, DMSO-d₆) δ 11.72, 11.63 (2s, 1H, OH/NH, D₂O exchangeable), 8.24, 8.03 (2s, 1H, CH=N), 8.09–8.06 (m, 1H, ArH), 7.86–7.78 (m, 1H, ArH), 7.73–7.66 (m, 4H, ArH), 7.61–7.54 (m, 2H, ArH), 7.49–7.45 (m, 4H, ArH), 7.11 (dd, $J=8.8, 2.0$ Hz, 2H, ArH), 7.06 (dd, $J=8.4, 4.0$ Hz, 2H, ArH), 4.47, 4.01 (2s, 2H, CH₂C=O); ¹³C NMR (100 MHz, DMSO-d₆) δ 169.1, 159.2, 158.3, 155.3, 147.5, 135.5, 135.3, 135.2, 131.9, 130.5, 130.2, 130.1, 129.5, 129.2, 128.4, 128.3, 127.1, 126.5, 126.5, 121.5, 121.4, 119.1, 118.9, 35.5, 34.7; Anal. Calcd for C₂₉H₂₀Cl₂N₄O₃S: C, 60.53; H, 3.50; N, 9.74, found C, 60.77; H, 3.68; N, 9.95; MS (ESI) m/z : 597 [M + Na⁺] and 599 [M + 2 + Na⁺].

N'-(4-(4-bromophenoxy)benzylidene)-2-((3-(4-chlorophenyl)-4-oxo-3,4-dihydroquinazolin-2-yl)thio)acetohydrazide (6e). Pale yellow solid: 89% yield; mp 138–140 °C; IR (KBr, cm⁻¹) 3448, 3182 (OH/NH), 3074 (CH aromatic), 2958, 2912 (CH aliphatic), 1681 (C=O), 1608 (C=N); ¹H NMR (400 MHz, DMSO-d₆) δ 11.71, 11.64 (2s, 1H, OH/NH, D₂O exchangeable), 8.24, 8.03 (2s, 1H, CH=N), 8.09–8.03 (m, 1H, ArH), 7.86–7.78 (m, 1H, ArH), 7.73–7.66 (m, 4H, ArH), 7.61–7.54 (m, 4H, ArH), 7.52–7.44 (m, 2H, ArH), 7.08–7.03 (m, 4H, ArH), 4.47, 4.01 (2s, 2H, CH₂C=O); ¹³C NMR (100 MHz, DMSO-d₆) δ

169.0, 163.8, 161.1, 161.1, 158.4, 158.2, 157.0, 156.8, 155.9, 155.8, 147.5, 146.5, 143.2, 135.4, 135.3, 135.2, 135.1, 133.4, 131.9, 130.1, 130.1, 129.5, 129.2, 127.1, 126.6, 126.5, 121.9, 121.7, 120.0, 119.9, 119.2, 119.0, 116.3, 116.2, 35.9, 34.8; Anal. Calcd for $C_{29}H_{20}BrClN_4O_3S$: C, 56.19; H, 3.25; N, 9.04, found C, 56.34; H, 3.49; N, 9.31; MS (ESI) m/z : 617 $[M - H]^-$ and 619 $[M + 2 - H]^-$.

2-((3-(4-chlorophenyl)-4-oxo-3,4-dihydroquinazolin-2-yl)thio)-N'-(4-(4-methoxy phenoxy)benzylidene)acetohydrazide (6f). White solid: 82% yield; mp 234–236 °C; IR (KBr, cm^{-1}) 3441, 3178 (OH/NH), 3070 (CH aromatic), 2970, 2939 (CH aliphatic), 1680 (C=O), 1608 (C=N); 1H NMR (400 MHz, DMSO- d_6) δ 11.68, 11.58 (2 s, 1H, OH/NH, D_2O exchangeable), 8.21, 8.00 (2 s, 1H, CH=N), 8.09–8.06 (m, 1H, ArH), 7.86–7.78 (m, 1H, ArH), 7.70–7.61 (m, 4H, ArH), 7.56 (t, $J=8.0$ Hz, 2H, ArH), 7.52–7.44 (m, 2H, ArH), 7.05 (d, $J=8.8$ Hz, 2H, ArH), 7.01–6.98 (m, 2H, ArH), 6.96–6.93 (m, 2H, ArH), 4.46, 4.00 (2 s, 2H, $CH_2C=O$), 3.78, 3.77 (2 s, 3H, OCH_3); ^{13}C NMR (100 MHz, DMSO- d_6) δ 169.0, 161.1, 160.1, 156.5, 149.0, 147.5, 143.4, 135.5, 135.2, 131.9, 130.1, 129.4, 129.1, 128.8, 127.1, 126.5, 121.8, 121.7, 119.9, 117.6, 117.5, 115.7, 55.9, 35.9, 34.7; Anal. Calcd for $C_{30}H_{23}ClN_4O_4S$: C, 63.10; H, 4.06; N, 9.81, found C, 63.28; H, 4.29; N, 9.97; MS (ESI) m/z : 593 $[M + Na]^+$ and 595 $[M + 2 + Na]^+$.

2-((4-oxo-3-phenyl-3,4-dihydroquinazolin-2-yl)thio)-N'-(4-(piperidin-1-yl)benzylidene)acetohydrazide (6g). Pale yellow solid: 78% yield; mp 164–166 °C; IR (KBr, cm^{-1}) 3441, 3178 (OH/NH), 3074 (CH aromatic), 2943, 2858 (CH aliphatic), 1681 (C=O), 1604 (C=N); 1H NMR (400 MHz, DMSO- d_6) δ 11.50, 11.39 (2 s, 1H, OH/NH, D_2O exchangeable), 8.10 (d, $J=2.4$ Hz, 1H, ArH), 8.08, 7.92 (2 s, 1H, CH=N), 7.85–7.78 (m, 1H, ArH), 7.62–7.59 (m, 3H, ArH), 7.53–7.45 (m, 6H, ArH), 6.93 (t, $J=8.0$ Hz, 2H, ArH), 4.45, 3.97 (2 s, 2H, $CH_2C=O$), 3.24 (brs, 4H, 2 CH_2 piperidine), 1.47 (brs, 6H, 3 CH_2 piperidine); ^{13}C NMR (100 MHz, DMSO- d_6) δ 168.8, 163.6, 161.2, 161.2, 157.4, 157.2, 152.8, 152.7, 147.8, 147.5, 144.5, 136.2, 136.1, 135.4, 130.5, 130.5, 130.1, 129.8, 128.9, 128.5, 127.0, 126.6, 126.5, 123.6, 123.4, 119.9, 115.1, 115.0, 48.9, 35.8, 34.7, 25.4, 24.4; Anal. Calcd for $C_{28}H_{27}N_5O_2S$: C, 67.58; H, 5.47; N, 14.07, found C, 67.40; H, 5.69; N, 14.31; MS (ESI) m/z : 520 $[M + Na]^+$.

N'-(4-morpholinobenzylidene)-2-((4-oxo-3-phenyl-3,4-dihydroquinazolin-2-yl)thio)acetohydrazide (6h). White solid: 91% yield; mp 236–242 °C; IR (KBr, cm^{-1}) 3479, 3224 (OH/NH), 3062 (CH aromatic), 2954, 2916 (CH aliphatic), 1681 (C=O), 1604 (C=N); 1H NMR (400 MHz, DMSO- d_6) δ 11.53, 11.43 (2 s, 1H, OH/NH, D_2O exchangeable), 8.12, 7.93 (2 s, 1H, CH=N), 8.08 (d, $J=7.6$ Hz, 1H, ArH), 7.86–7.79 (m, 1H, ArH), 7.62–7.59 (m, 4H, ArH), 7.55–7.52 (m, 2H, ArH), 7.50–7.45 (m, 3H, ArH), 6.97 (t, $J=7.6$ Hz, 2H, ArH), 4.45, 3.97 (2 s, 2H, $CH_2C=O$), 3.73 (q, $J=4.8$ Hz, 4H, 2 CH_2 morpholine), 3.20 (t, $J=4.8$ Hz, 4H, 2 CH_2 morpholine); ^{13}C NMR (100 MHz, DMSO- d_6) δ 168.8, 163.6, 161.1, 157.5, 152.7, 152.5, 147.6, 144.2, 136.3, 136.2, 135.4, 130.4, 130.0, 129.9, 128.8, 128.4, 127.1, 126.5, 124.8, 124.7, 119.9, 114.9, 114.8, 66.4, 48.0, 47.9, 35.8, 34.7; Anal. Calcd for $C_{27}H_{25}N_5O_3S$: C, 64.91; H, 5.04; N, 14.02; found C, 64.75; H, 5.23; N, 14.29; MS (ESI) m/z : 522 $[M + Na]^+$.

N'-(4-(4-methylpiperazin-1-yl)benzylidene)-2-((4-oxo-3-phenyl-3,4-dihydroquinazolin-2-yl)thio)acetohydrazide (6i). Pale yellow solid: 82% yield; mp 120–122 °C; IR (KBr, cm^{-1}) 3441, 3163 (OH/NH), 3074 (CH aromatic), 2943, 2862 (CH aliphatic), 1681 (C=O), 1604 (C=N); 1H NMR (400 MHz, DMSO- d_6) δ 11.53, 11.42 (2 s, 1H, OH/NH, D_2O exchangeable), 8.12, 7.93 (2 s, 1H, CH=N), 8.08 (d,

$J=7.2$ Hz, 1H, ArH), 7.88–7.76 (m, 2H, ArH), 7.59 (brs, 4H, ArH), 7.52–7.48 (m, 4H, ArH), 6.95–6.94 (m, 2H, ArH), 4.45, 3.97 (2 s, 2H, $CH_2C=O$), 3.23 (brs, 4H, 2 CH_2 piperazine), 2.45 (brs, 4H, 2 CH_2 piperazine), 2.22 (s, 3H, NCH_3); ^{13}C NMR (100 MHz, DMSO- d_6) δ 172.6, 168.8, 163.5, 161.2, 161.1, 157.5, 157.3, 152.5, 152.4, 147.6, 144.3, 136.3, 136.2, 135.4, 130.5, 130.4, 130.0, 129.9, 128.8, 128.4, 127.1, 126.5, 126.4, 124.4, 124.3, 120.0, 115.0, 114.9, 54.8, 47.5, 47.4, 46.1, 35.9, 34.8, 21.6; Anal. Calcd for $C_{28}H_{28}N_6O_2S$: C, 65.60; H, 5.51; N, 16.39; found C, 65.43; H, 5.67; N, 16.58.

2-((3-(4-chlorophenyl)-4-oxo-3,4-dihydroquinazolin-2-yl)thio)-N'-(4-(piperidin-1-yl)benzylidene)acetohydrazide (6j). Pale yellow solid: 85% yield; mp 242–244 °C; IR (KBr, cm^{-1}) 3448, 3178 (OH/NH), 3089 (CH aromatic), 2935, 2854 (CH aliphatic), 1681 (C=O), 1604 (C=N); 1H NMR (400 MHz, DMSO- d_6) δ 11.49, 11.41 (2 s, 1H, OH/NH, D_2O exchangeable), 8.09 (s, 1H, ArH), 8.07, 7.90 (2 s, 1H, CH=N), 7.86–7.80 (m, 1H, ArH), 7.68 (dd, $J=8.4$, 2.8 Hz, 2H, ArH), 7.62–7.54 (m, 3H, ArH), 7.51–7.46 (m, 3H, ArH), 6.96–6.92 (m, 2H, ArH), 4.45, 3.99 (2 s, 2H, $CH_2C=O$), 3.26 (brs, 4H, 2 CH_2 piperidine), 1.58 (brs, 6H, 3 CH_2 piperidine); ^{13}C NMR (100 MHz, DMSO- d_6) δ 168.6, 163.3, 161.1, 161.1, 157.1, 156.9, 152.8, 152.7, 147.8, 147.5, 144.4, 135.5, 135.2, 135.2, 135.2, 135.1, 131.9, 130.1, 130.1, 128.9, 128.5, 127.1, 126.6, 126.5, 123.6, 123.5, 119.9, 115.1, 115.0, 48.9, 48.8, 35.9, 34.8, 25.4, 24.4; Anal. Calcd for $C_{28}H_{26}ClN_5O_2S$: C, 63.21; H, 4.93; N, 13.16; found C, 63.40; H, 5.19; N, 13.46; MS (ESI) m/z : 554 $[M + Na]^+$.

2-((3-(4-chlorophenyl)-4-oxo-3,4-dihydroquinazolin-2-yl)thio)-N'-(4-morpholino benzylidene)acetohydrazide (6k). White solid: 75% yield; mp 240–242 °C; IR (KBr, cm^{-1}) 3444, 3255 (OH/NH), 3097 (CH aromatic), 2962, 2858 (CH aliphatic), 1666 (C=O), 1604 (C=N); 1H NMR (400 MHz, DMSO- d_6) δ 11.53, 11.45 (2 s, 1H, OH/NH, D_2O exchangeable), 8.12, 7.93 (2 s, 1H, CH=N), 8.08 (d, $J=8.0$ Hz, 1H, ArH), 7.86–7.79 (m, 1H, ArH), 7.69–7.67 (m, 2H, ArH), 7.57–7.55 (m, 2H, ArH), 7.54–7.50 (m, 3H, ArH), 7.48–7.46 (m, 1H, ArH), 6.99–6.96 (m, 2H, ArH), 4.46, 3.99 (2 s, 2H, $CH_2C=O$), 3.73 (q, $J=4.8$ Hz, 4H, 2 CH_2 morpholine), 3.20 (t, $J=4.8$ Hz, 4H, 2 CH_2 morpholine); ^{13}C NMR (100 MHz, DMSO- d_6) δ 168.7, 163.4, 161.1, 157.2, 152.7, 152.5, 147.5, 144.2, 135.5, 135.2, 135.2, 131.9, 130.1, 128.8, 128.4, 127.1, 126.5, 124.8, 119.9, 114.9, 114.8, 66.4, 48.0, 47.9, 40.6, 35.9, 34.8; Anal. Calcd for $C_{27}H_{24}ClN_5O_3S$: C, 60.72; H, 4.53; N, 13.11; found C, 60.98; H, 4.31; N, 13.40; MS (ESI) m/z : 532 $[M - H]^-$ and 534 $[M + 2 - H]^-$.

2-((3-(4-chlorophenyl)-4-oxo-3,4-dihydroquinazolin-2-yl)thio)-N'-(4-(4-methylpiperazin-1-yl)benzylidene)acetohydrazide (6l). White solid: 86% yield; mp 204–206 °C; IR (KBr, cm^{-1}) 3444, 3167 (OH/NH), 3078 (CH aromatic), 2939, 2843 (CH aliphatic), 1674 (C=O), 1604 (C=N); 1H NMR (400 MHz, DMSO- d_6) δ 11.52, 11.43 (2 s, 1H, OH/NH, D_2O exchangeable), 8.11, 7.92 (2 s, 1H, CH=N), 8.08 (d, $J=7.6$ Hz, 1H, ArH), 7.86–7.79 (m, 1H, ArH), 7.68 (dd, $J=8.4$, 2.4 Hz, 2H, ArH), 7.57–7.54 (m, 2H, ArH), 7.53–7.45 (m, 4H, ArH), 6.97–6.94 (m, 2H, ArH), 4.46, 3.99 (2 s, 2H, $CH_2C=O$), 3.23 (brs, 4H, 2 CH_2 piperazine), 2.45–2.43 (m, 4H, 2 CH_2 piperazine), 2.22, 2.21 (2 s, 3H, NCH_3); ^{13}C NMR (100 MHz, DMSO- d_6) δ 168.7, 163.3, 161.1, 161.1, 157.2, 156.9, 152.6, 152.4, 147.6, 147.5, 144.3, 135.5, 135.2, 135.2, 135.1, 131.9, 130.1, 130.1, 128.8, 128.4, 127.1, 126.6, 126.5, 124.3, 124.2, 120.0, 119.9, 115.0, 114.9, 54.9, 47.6, 47.5, 46.2, 35.9, 34.9; Anal. Calcd for $C_{28}H_{27}ClN_6O_2S$: C, 61.47; H, 4.97; N, 15.36; found C, 61.39; H, 5.13; N, 15.58; MS (ESI) m/z : 547 $[M + H]^+$ and 549 $[M + 2 + H]^+$.

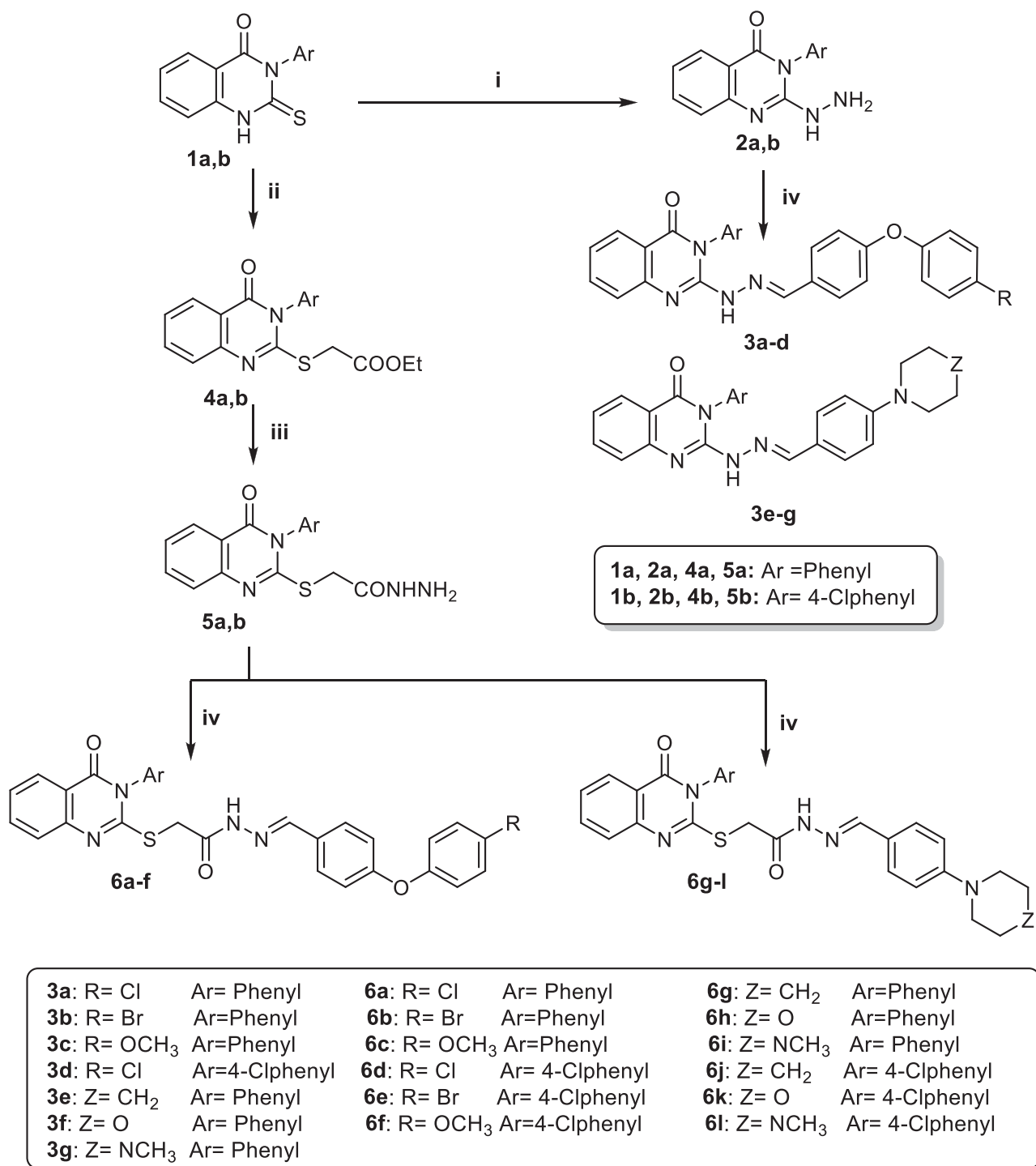
Biological evaluation

Biological assays

The biological assays were carried out according to the previously reported procedures and have been provided in the [Supplementary Materials](#); antiproliferative activity screening and five dose concentrations assay by NCI^{34–37}, *in vitro* EGFR inhibitory assay³⁸, cell cycle analysis³⁹, apoptosis assay⁴⁰, caspase-3 enzyme assay⁴¹.

Molecular modelling studies

The crystallographic structure of EGFR protein (PDB: 1M17) was obtained from the protein data bank website, (<http://www.pdb.org>) with resolution of 2.60 Å. All the molecular modelling studies were carried out using Molecular Operating Environment (MOE 2020.09; Chemical Computing Group, Canada) as the computational software. The hydrogen atoms were added, the protonation states of the amino acid residues were assigned, and the partial charges of atoms



Scheme 1. Synthesis of quinazolin-4(3*H*)-one derivatives **3a–g** and **6a–l**. **Reagents and conditions:** (i) NH₂NH₂·H₂O, ethanol, reflux, 12 h; (ii) Ethyl bromoacetate, dry acetone, anhydrous K₂CO₃, RT, 8 h; (iii) NH₂NH₂·H₂O, ethanol, reflux, 6 h; (iv) 4-Substituted benzaldehyde, ethanol, drops of glacial acetic acid, reflux, 6 h.

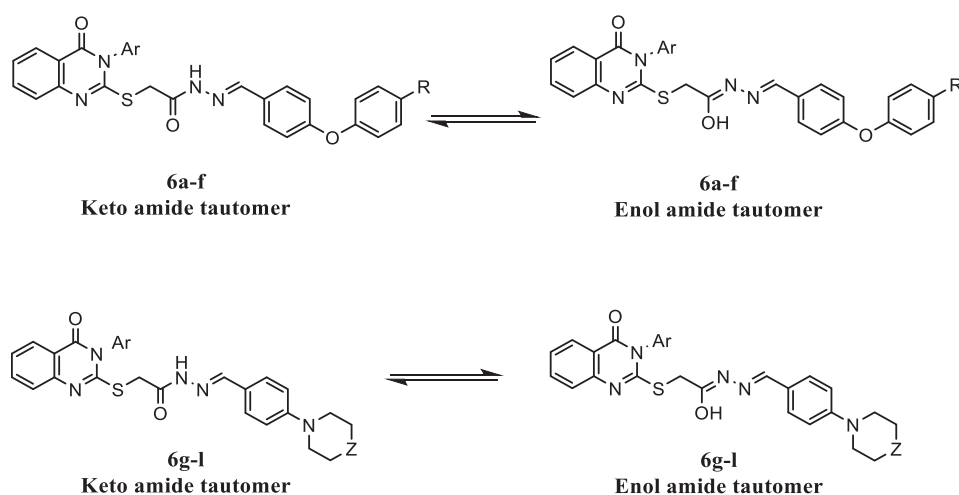


Figure 3. Tautomerism in hydrazone derivatives **6a–f** and **6g–l**.

were added using Protonate 3D algorithm. Compounds were modelled using MOE builder, and the structure was energy minimised using the MMFF94x force field. Using the MOE induced-fit Dock tool, docking studies of the synthesised compound into the active site was done and the final docked complexes of ligand–enzyme was selected according to the criteria of binding energy score combined with geometrical matching quality.

Statistical analysis

Data are represented as mean \pm SD. Significant differences between groups were analysed by using Graphpad Prism 9.1.0. Differences were considered significant at $p < 0.05$.

Result and discussion

Chemistry

Nineteen new quinazolin-4(3H)-one derivatives **3a–g** and **6a–l** were synthesised according to Scheme 1. The key starting compounds 3-phenyl-2-thioxo-2,3-dihydroquinazolin-4(1H)-one (**1a**) and 3-(4-chlorophenyl)-2-thioxo-2,3-dihydroquinazolin-4(1H)-one (**1b**) were obtained in good yields by reacting anthranilic acid with the appropriate aryl isothiocyanate in refluxing ethanol in presence of triethylamine as catalyst^{30,31}. Compounds **1a,b** were then treated with hydrazine hydrate 99% as reported to yield 2-hydrazinyl-3-phenylquinazolin-4(3H)-one (**2a**) and 3-(4-chlorophenyl)-2-hydrazinylquinazolin-4(3H)-one (**2b**)³¹. Furthermore, heating the obtained hydrazine derivatives **2a,b** with 4-substituted benzaldehyde derivatives in ethanol as solvent in the presence of few drops of glacial acetic acid⁴² afforded the novel target compounds **3a–g**. The ¹H NMR spectra of the compounds **3a–g** showed D₂O exchangeable singlet signal due to NH at the range δ 10.49–10.61 ppm. Moreover, singlet signal at the range δ 7.93–8.09 ppm was present due to the characteristic azomethine protons.

On the other hand, alkylation of 2-thioxo-2,3-dihydroquinazolin-4(1H)-one derivatives **1a,b** with ethyl bromoacetate at room temperature in dry acetone containing anhydrous potassium carbonate afforded ethyl 2-((4-oxo-3-aryl-3,4-dihydroquinazolin-2-yl)thio)acetate **4a,b**^{32,33}. The ester derivatives **4a,b** were further reacted with hydrazine hydrate 99% to afford the corresponding acetohydrazide derivatives 2-((4-oxo-3-aryl-3,4-dihydroquinazolin-

2-yl)thio)acetohydrazide **5a,b**^{32,33}. Compounds **5a,b** were finally reacted with 4-substituted benzaldehyde derivatives to yield the desired hydrazone derivatives **6a–l**. The ¹H NMR spectra of derivatives **6a–l** revealed that the hydrazones existed in a keto amide/enol amide mixture (Figure 3)⁴³. ¹H NMR spectra of series **6a–l** showed two singlet signals with an integration of 2H due to $\text{SCH}_2\text{C}=\text{O}$ protons at the ranges of δ 4.45–4.47 ppm and δ 3.97–4.01 ppm corresponding to keto amide and enol amide tautomers, respectively. Moreover, two singlet signals with an integration of 1H in ¹H NMR spectra of **6a–l** appeared due to the azomethine protons of both tautomers at the ranges of δ 8.07–8.24 and δ 7.90–8.04 ppm. Additionally, two D₂O exchangeable peaks due to OH proton in enol and NH in keto tautomers with 1H total integration appeared at the ranges of δ 11.49–11.73 ppm and δ 11.39–11.64 ppm, respectively. On the other hand, the appearance of the OCH₃ group in derivatives **6c** and **6f** as two singlet signals with total integration of 3H at δ 3.77–3.78 ppm and δ 3.76–3.77 ppm is in concordance with the presence of tautomerism. ¹³C NMR spectra of derivatives **6a–l** showed two peaks at the ranges δ 35.8–35.9 ppm and δ 34.6–34.9 ppm corresponding to $\text{SCH}_2\text{C}=\text{O}$ in enol and keto tautomers, respectively.

Biological evaluation

Evaluation of antiproliferative activity against a panel of 60 human cancer cell lines

Two series of substituted quinazolinone derivatives **3a–g** and **6a–l** were evaluated for their antiproliferative activity at a single dose (10 μM) using 60 human cancer cell lines, by the National Cancer Institute (NCI), USA. The screening was achieved under the Developmental Therapeutic Program (DTP)^{34–37}. NCI cell lines include leukaemia, melanoma, and cancers of the breast, kidney, ovarian, colon, central nervous system (CNS), prostate, and non-small cell (NSC) lung. The growth inhibition percentage (GI%) representing the *in vitro* antiproliferative activity was illustrated in Table 1.

The series **3a–g**, representing 2-(substitutedbenzylidene)hydrazinyl quinazolin-4(3H)-ones showed low to no activity against most of the investigated cancer cell lines (Supplementary data). In contrast, five derivatives of the acetohydrazide series **6a–l** displayed potent broad-spectrum antiproliferative activity against

Table 1. *In vitro* growth inhibition % (GI%) of the synthesised compounds **6a–6l** against a panel of 60 tumour cell lines at 10 μ M.

Subpanel	6a	6b	6c	6d	6e	6f	6g	6h	6i	6j	6k	6l
Leukaemia												
CCRF-CEM	49.57	43.1	–	> 100	–	36.46	–	–	–	–	–	–
HL-60(TB)	–	–	–	–	–	–	–	–	–	–	–	–
K-562	38.79	37.52	–	77.02	–	41.57	26.76	–	–	26.42	–	–
MOLT-4	41.34	44.47	–	> 100	–	38.29	28.47	–	–	–	–	–
RPMI-8226	26.75	31.73	–	75.28	–	14.91	17.56	–	–	–	–	–
SR	29.66	26.64	–	67.08	–	27.19	24.73	–	–	25.23	–	–
NSC lung cancer												
A549/ATCC	58.27	57.81	–	83.53	–	52.97	15.14	–	–	50.65	–	–
EKVX	40.95	39.26	–	59.16	–	30.59	20.43	–	–	17.94	–	–
HOP-62	40.92	36.11	–	67.44	–	26.68	–	–	–	81.63	–	–
HOP-92	33.3	26.96	–	97.41	–	22.66	19.49	18.69	–	37.67	–	–
NCI-H226	27.88	22.43	–	24.44	–	20.29	–	–	–	61.77	–	–
NCI-H322M	15.51	–	–	–	–	15.35	–	–	–	23.03	–	–
NCI-H460	67.86	71.98	–	> 100	–	88.8	–	–	–	90.26	–	–
NCI-H522	50.38	51.53	–	79.34	13.4	48.7	15.3	–	–	–	–	–
Colon cancer												
COLO-205	50.76	55.61	–	85.4	–	27.18	–	–	–	17.87	–	–
HCC-2998	–	–	–	79.7	–	16.65	–	–	–	–	–	–
HCT-116	94.38	92.19	–	> 100	–	86.66	15.51	–	–	63.1	–	–
HCT-15	39.16	36.28	–	89.62	–	43.95	16.21	–	–	32.2	–	–
HT29	40.85	61.82	–	98.24	–	83.93	–	–	–	39.1	–	–
KM12	16.31	23.73	–	82.6	–	22.83	–	–	–	3.59	–	–
SW-620	56.93	70.37	–	97.38	–	55.6	–	–	–	34.12	–	–
CNS cancer												
SF-268	–	15.72	–	44.24	–	42.06	–	–	–	65.26	–	–
SF-295	16.22	16.28	–	35.28	–	32.32	–	–	–	23.56	–	–
SF-539	31.48	31.3	–	30.33	–	67.83	–	–	–	58.67	–	–
SNB-19	66.78	60.15	–	71.51	–	38.45	–	–	–	56.75	–	–
SNB-75	39.91	42.17	–	42.06	–	58.37	19.86	–	–	20.14	–	–
U251	84.83	78.53	–	> 100	–	63.53	–	–	–	49.41	–	–
Melanoma												
LOX IMIV	86.02	79.01	–	> 100	–	85.33	–	–	–	56.49	–	15.15
MALME-3M	48.74	45.07	–	> 100	–	36.13	–	–	–	35.79	–	–
M14	51.16	43.73	NT	> 100	NT	NT	–	NT	NT	NT	NT	NT
MDA-MB-435	15.38	19.23	–	74.95	–	–	–	–	–	–	–	–
SK-MEL-2	13.13	–	–	45.68	–	–	–	–	–	–	–	–
SK-MEL-28	37.58	29.11	–	96.83	–	–	–	–	–	15.16	–	–
SK-MEL-5	28.84	40.93	–	89.11	–	21.98	–	–	–	–	–	–
UACC-257	–	–	–	41.0	–	–	–	–	–	–	–	–
UACC-62	33.42	31.24	–	99.57	–	38.11	–	–	–	26.53	–	–
Ovarian cancer												
IGROV1	50.89	34.45	–	79.42	–	51.35	–	–	–	44.51	–	–
OVCAR-3	–	–	–	–	–	> 100	–	–	–	67.19	–	–
OVCAR-4	26.25	18.26	–	98.3	–	27.45	–	–	–	41.44	–	–
OVCAR-5	18.55	–	–	29.36	–	18.76	–	–	–	23.12	–	–
OVCAR-8	40.84	36.67	–	86.57	–	–	–	–	–	34.7	–	–
NCI/ADR-RES	47.27	44.83	–	84.26	–	48.89	–	–	–	60.15	–	–
SK-OV-3	16.8	15.49	–	66.17	–	33.7	–	–	–	69.91	–	–
Renal cancer												
786-0	46.79	54.01	–	> 100	–	74.84	–	–	–	92.8	–	–
A498	34.29	17.71	17.18	> 100	15.7	27.11	–	15.82	10.22	21.52	–	32.61
ACHN	25.52	–	–	36.52	–	92.17	–	–	–	82.62	–	–
CAKI-1	40.81	29.24	NT	66.99	NT	NT	21.97	NT	NT	NT	NT	NT
RXF 393	57.96	37.84	NT	> 100	NT	NT	–	NT	NT	NT	NT	NT
SN12C	73.08	59.26	–	54.75	–	47.29	–	–	–	37.62	–	–
TK-10	–	–	–	60.33	–	–	–	–	–	–	–	–
UO-31	18.82	–	–	–	20.82	52.26	23.31	–	–	46.97	–	–
Prostate cancer												
PC-3	41.33	28.25	–	99.2	–	36.32	18.52	–	–	21.44	–	–
DU-145	61.56	61.67	–	86.91	–	50.84	–	–	–	70.89	–	–
Breast cancer												
MCF7	35.46	31.12	–	84.47	–	50.72	16.22	–	–	32.51	–	–
MDA-MB-231/ATCC	50.77	49.15	–	69.61	–	53.27	–	–	–	28.05	–	–
HS 578T	41.12	39.2	–	78.62	–	> 100	–	–	–	62.12	–	–
BT-549	30.09	26.93	–	> 100	–	–	–	–	–	–	–	–
T-47D	17.5	17.61	–	69.86	–	62.15	–	–	–	25.43	–	–
MDA-MB-468	28.41	34.89	–	> 100	–	33.16	–	–	–	20.54	–	–
Mean	37.29	34.78	< 0	80.23	< 0	42.46	4.28	< 0	< 0	34.19	< 0	< 0

–: growth inhibition below 15%; NT: not tested.

Bold numbers: growth inhibition above 70%.

most of the examined cancer cell lines with mean growth percentage of range 34.19 – 80.23%.

4-chlorophenoxybenzylidene acetohydrazide derivative **6a** exhibited broad-spectrum antiproliferative activity with mean GI% of 37.29. It showed significantly potent antiproliferative activity against colon cancer HCT-116 (GI% 94.38); CNS cancer U251 (GI% 84.83); melanoma LOX IMIV (GI% 86.02) and renal cancer SN12C (GI% 73.08). It had also demonstrated excellent-to-moderate antiproliferative activity against 33 cancer cell lines with GI% in the range of 67.86% to 30.09%. Moreover, compound **6b** with 4-bromophenoxybenzylidene acetohydrazide demonstrated broad-spectrum antiproliferative activity with mean growth inhibition of 34.78%. It showed significantly potent antiproliferative activity against NSC lung cancer NCI-H460; colon cancer (HCT-116 and SW-620); CNS cancer U251 and melanoma LOX IMIV with GI% 71.98%, 92.19%, 70.37%, 78.53% and 79.01%, respectively. It revealed excellent-to-moderate antiproliferative activity against 29 cancer cell lines with growth inhibition in the range of 61.82–31.2%.

Compound **6c** with 4-methoxyphenoxy substitution showed no activity against all tested cancer cell lines. Compound **6d** with (4-chlorophenoxy)benzylidene-3-(4-chlorophenyl)quinazolinone demonstrated significantly potent to excellent broad-spectrum antiproliferative activity with mean GI% 80.23. It was accordingly evaluated at five dose concentrations by NCI to define its dose-response behaviour and determine its GI₅₀, TGI, and LC₅₀ values. (Values were represented in Table 2). Compound **6d** showed significantly potent antiproliferative activity against 24 cancer cell lines with GI% ranging between 99.57% and 71.51%. Also, compound **6d** showed significantly potent antiproliferative activity with inhibition percentage above 90% with NSC lung cancer HOP-92 (GI% 97.41); colon cancer (HT29 and SW-620 with GI% 98.24 and 97.38, respectively); melanoma (SK-MEL-28 and UACC-62 with GI% 96.83 and 99.57 respectively); ovarian cancer OVCAR-4 (GI% 98.3) and prostate cancer PC-3 (GI% 99.2). Additionally, compound **6d** displayed lethal activity against 13 of the tested cancer cell lines with growth inhibition above 100%.

Replacing 4-chlorophenoxy with 4-bromophenoxy in derivative **6e** resulted in abolishing the antiproliferative activity. On the other hand, derivative **6f** with 4-methoxyphenoxy substitution displayed antiproliferative activity (mean GI% of 42.46). Compound **6f** exhibited significantly potent antiproliferative activity against 6 cancer cell lines representing NSC lung cancer NCI-H460; colon cancer (HCT-116 and HT29); melanoma LOX IMIV and renal cancer (786-0 and ACHN) with GI% 88.8%, 86.66%, 83.93%, 85.33%, 74.84% and 92.17%, respectively. It also showed moderate activity against 27 cell lines with growth inhibition percentage ranging from 67.83 to 30.59%. In addition, compound **6f** showed lethal activity against ovarian cancer OVCAR-3 and breast cancer HS 578T with growth inhibition above 100%.

Derivative **6j** with *N'*-(4-(piperidin-1-yl)benzylidene)-3-(4-chlorophenyl)-quinazolinone acetohydrazide showed antiproliferative activity with mean GI% of 34.19. It showed significantly potent antiproliferative activity against 5 cell lines including NSC lung cancer (HOP-62 and NCI-H460); renal cancer (786-0 and ACHN) and prostate DU-145 with GI% 81.63%, 90.26%, 92.8%, 82.62% and 70.89% respectively. It showed moderate antiproliferative activity against 23 cell lines with GI% range of 69.91–32.2%. Finally, derivatives **6h**, **6i**, **6k** and **6l** did not show activity against all cell lines.

Table 2. The values of GI₅₀, TGI and LC₅₀ of compound **6d** at 5 doses against 60 cell line panel.

Compound	6d		
	GI ₅₀	TGI	LC ₅₀
Leukaemia			
CCRF-CEM	3.09	48.5	>100
HL-60(TB)	16.0	37.0	85.7
K-562	4.15	20.2	>100
MOLT-4	2.29	9.23	44.7
RPMI-8226	2.98	15.8	>100
SR	1.84	6.86	31.9
NSC lung cancer			
A549/ATCC	3.25	14.0	83.3
EKVX	3.1	13.9	63.6
HOP-62	1.69	4.05	9.69
HOP-92	2.07	5.62	22.8
NCI-H226	2.46	6.59	33.2
NCI-H322M	3.02	15.0	90.8
NCI-H460	0.789	2.6	7.78
NCI-H522	2.34	8.31	42.6
Colon cancer			
COLO 205	2.79	8.74	91.6
HCC-2998	1.92	3.81	7.57
HCT-116	1.55	3.74	9.03
HCT-15	2.41	7.48	28.5
HT29	2.14	11.1	>100
KM12	2.04	5.0	26.6
SW-620	1.81	7.84	42.4
CNS cancer			
SF-268	3.85	23.9	>100
SF-295	3.61	13.3	36.4
SF-539	2.54	6.32	21.5
SNB-19	3.36	12.7	53.2
SNB-75	3.99	29.2	>100
U251	1.65	3.69	8.23
Melanoma			
LOX IMVI	1.29	2.59	5.2
MALME-3M	1.38	2.77	5.55
M14	1.58	3.47	7.58
MDA-MB-435	1.93	4.56	13.0
SK-MEL-2	2.86	8.93	41.3
SK-MEL-28	1.51	3.01	6.01
SK-MEL-5	1.75	3.51	7.07
UACC-257	4.62	22.5	>100
UACC-62	1.59	3.18	6.38
Ovarian cancer			
IGROV1	1.51	3.28	7.12
OVCAR-3	2.75	9.55	38.9
OVCAR-4	1.89	4.57	17.5
OVCAR-5	2.27	6.44	32.2
OVCAR-8	2.41	6.56	>100
NCI/ADR-RES	1.64	3.56	7.76
SK-OV-3	3.26	11.9	49.4
Renal cancer			
786-0	2.51	6.41	26.5
A498	1.94	4.34	9.74
ACHN	4.36	15.2	39.0
CAKI-1	3.06	12.0	35.4
RXF 393	1.7	3.14	5.81
SN12C	1.74	4.14	9.84
TK-10	5.97	40.2	>100
UO-31	7.47	21.1	47.1
Prostate cancer			
PC-3	2.58	9.32	>100
DU-145	3.52	20.4	>100
Breast cancer			
MCF7	2.01	5.5	25.6
MDA-MB-231/ATCC	1.79	3.9	8.51
HS 578T	2.17	6.36	>100
BT-549	3.28	12.2	36.2
T-47D	2.09	5.76	49.5
MDA-MB-468	2.08	5.08	18.8

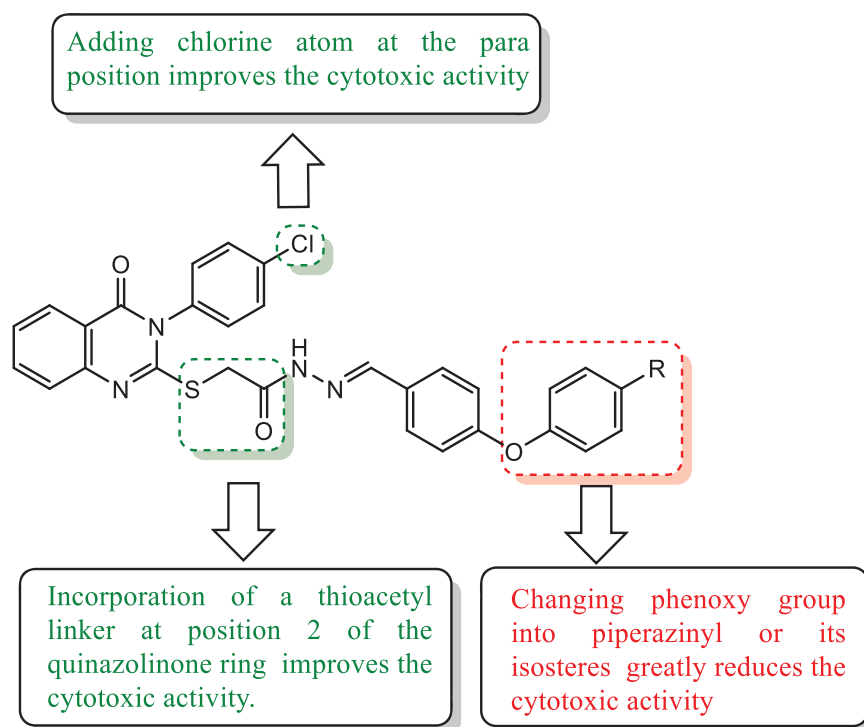


Figure 4. Structure activity relationship for synthesised quinazolinone derivatives correlated with their cytotoxic activity.

Table 3. EGFR kinase inhibitory activity of compounds **6a**, **6b**, **6d**, **6f** and **6j** compared with erlotinib

Compound	EGFR IC ₅₀ (μM ± SD) ^a
6a	0.202 ± 0.012
6b	0.487 ± 0.030
6d	0.069 ± 0.004
6f	0.133 ± 0.008
6j	0.478 ± 0.029
Erlotinib	0.045 ± 0.003

^aIC₅₀ are presented as mean of three independent experiments.

The most remarkable effects to be concluded in the structure variations of the synthesised derivatives and their antiproliferative activity are represented in Figure 4. The incorporation of thioacetyl linker at position 2 of the quinazolinone ring was found to be essential for the antiproliferative activity as most of the synthesised compounds with thioacetyl bridge in series **6a–l** were found to have of high anticancer activity while compounds **3a–g**, lacking the thioacetyl bridge, showed no promising results. This may be due to the increased flexibility introduced by thioacetyl spacer, which enables the compounds to fit better into the receptor⁴⁴.

In series **6a–l**, general better antiproliferative activity were displayed by compounds bearing chloro atom at the para-position of the quinazolinone 3-phenyl ring as demonstrated by the relatively high GI percentage values of compounds **6d** (mean GI% = 80.23%), **6f** (mean GI% = 42.46%) and **6j** (mean GI% = 34.19%) over their unsubstituted analogues **6a** (mean GI% = 37.29%), **6c** (mean GI% = 0%) and **6g** (mean GI% = 4.28%), respectively. This observation was in accordance with the previously reported study in other related compounds⁴⁵. It was also observed that the substituted phenoxy derivatives **6a–f** have generally better GI% values than the corresponding piperazinyl (or its isostere) aryl group **6g–l**.

Evaluation of in vitro antiproliferative activity of compound **6d** at 5 dose concentrations

Compound **6d** was found to be the most effective anticancer agent in this study based on preliminary single dose (10 μM)

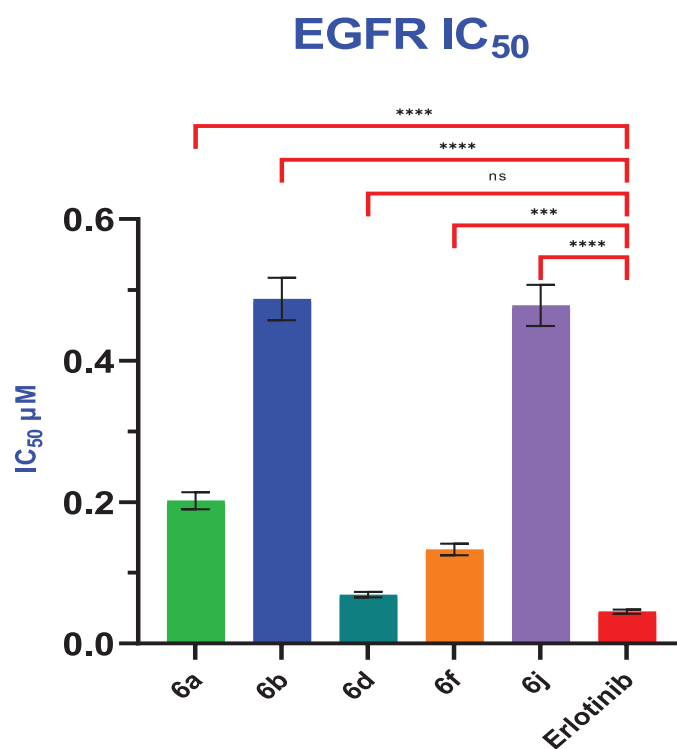


Figure 5. Graphical illustration for IC₅₀ inhibition of EGFR of compounds **6a**, **6b**, **6d**, **6f** and **6j** compared to erlotinib. Statistical significance was analysed by one-way ANOVA and Tukey's multiple comparisons test (ns: non-significant, ****p* < 0.001, *****p* < 0.0001).

screening results. It demonstrated promising efficacy against a variety of cancer cell lines, with mean growth inhibition of 80.23% (Table 1). Accordingly, compound **6d** was further subjected to five dose concentrations assay (0.01, 0.1, 1, 10 and

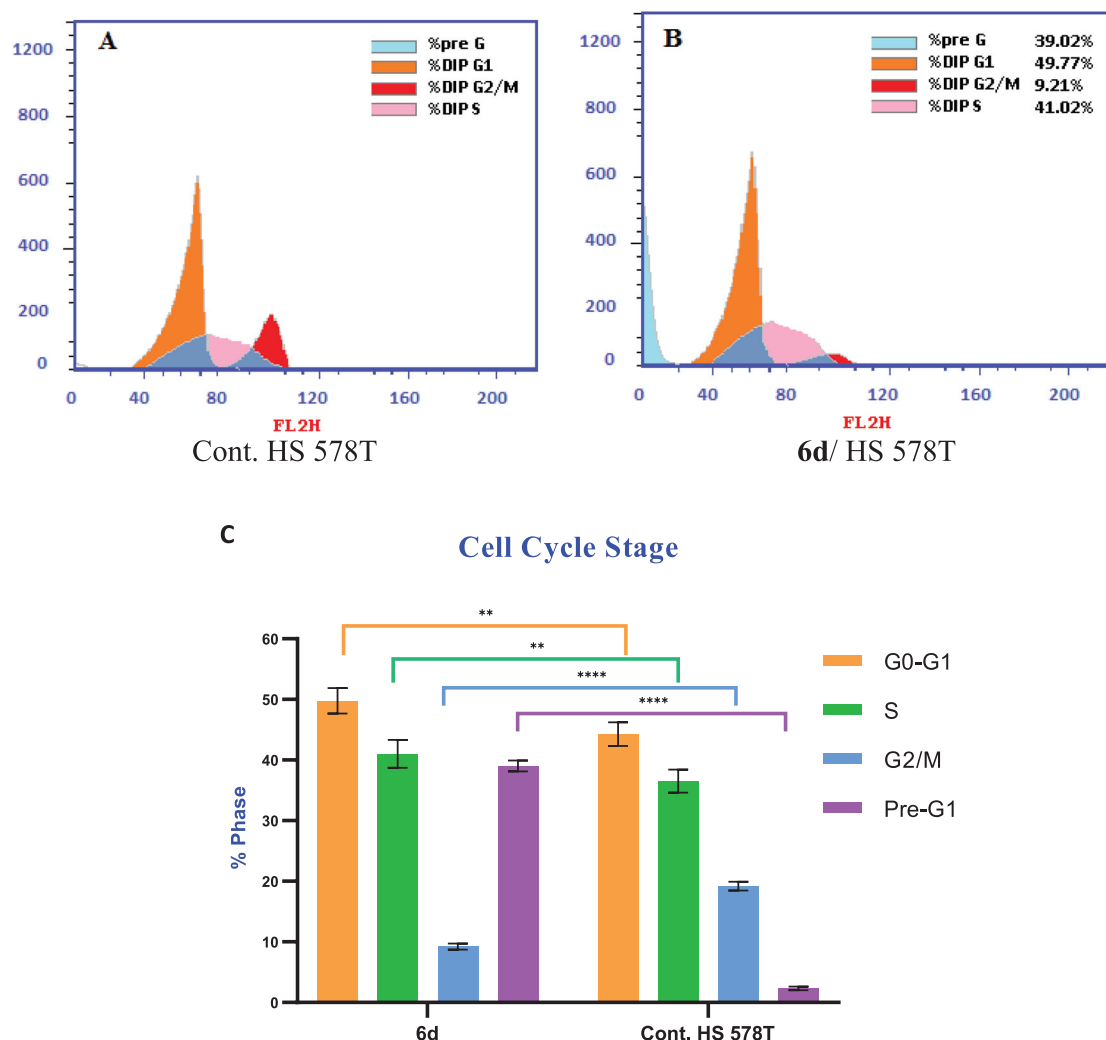


Figure 6. Cell cycle analysis in breast HS 578T cell line. (A) Control HS 578T; (B) Treatment with **6d**; (C) Graphical diagram for distribution of cell cycle analysis in treated and untreated control cells. Statistical significance was analysed by two-way ANOVA and Tukey's multiple comparisons test (** $p < 0.01$, **** $p < 0.0001$).

100 μM) to detect its dose-response behaviour and calculate the values of GI_{50} (the dose that inhibit 50% of cell growth in comparison to control), TGI (the dose that completely inhibit growth), and LC_{50} (the dose that kill 50% of the cells). The values are presented in Table 2. The obtained results showed that, compound **6d** displayed superior sub-micromolar activity towards NSC lung cancer cell line NCI-H460 with $\text{GI}_{50} = 0.789 \mu\text{M}$, however it showed high lethality with this cell line ($\text{LC}_{50} = 7.78 \mu\text{M}$). Compound **6d** exhibited also potent and broad-spectrum antiproliferative activity against most of the tested cancer cell lines, with GI_{50} values in the range of 1.29–5.97 μM , in addition to moderate antiproliferative activity against leukaemia cell line HL-60(TB) with $\text{GI}_{50} = 16.0 \mu\text{M}$. Compound **6d** also exhibited high cytostatic activity (TGI range: 2.59–9.55 μM) against 40 cancer cell lines. Moreover, **6d** demonstrated good to moderate cytostatic activity against the rest of cell lines with TGI range of 11.1–48.5 μM . Compound **6d** exhibited remarkable differences between its cytotoxic indicator (LC_{50}) and cytostatic markers (GI_{50} and TGI) against colon cancer HT29; ovarian cancer OVCAR-8; prostate cancer PC-3 and breast cancer HS 578T, which indicates a wide therapeutic index.

Table 4. Annexin V/PI dual staining assay in breast HS 578T cells; Distribution of apoptotic cells after treatment with compound **6d**.

Comp.	Apoptosis			Necrosis
	Total	Early	Late	
6d	39.02	19.24	13.45	6.33
Control	2.33	0.37	0.22	1.74

In vitro EGFR kinase inhibitory assay

The most potent compounds **6a**, **6b**, **6d**, **6f** and **6j**, with promising antiproliferative activity with mean inhibition range of 34.19–80.23%, were assayed for their EGFR inhibition. The results were summarised in Table 3 and Figure 5 as 50% inhibition concentration value (IC_{50}) calculated from the concentration inhibition response curve. In this assay, erlotinib is used as positive control. Compound **6d** potentially inhibited EGFR with $\text{IC}_{50} = 0.069 \pm 0.004 \mu\text{M}$ in comparison to erlotinib with IC_{50} value of $0.045 \pm 0.003 \mu\text{M}$. It was obvious that there was non-significant difference between IC_{50} values scored by both compound **6d** and erlotinib.

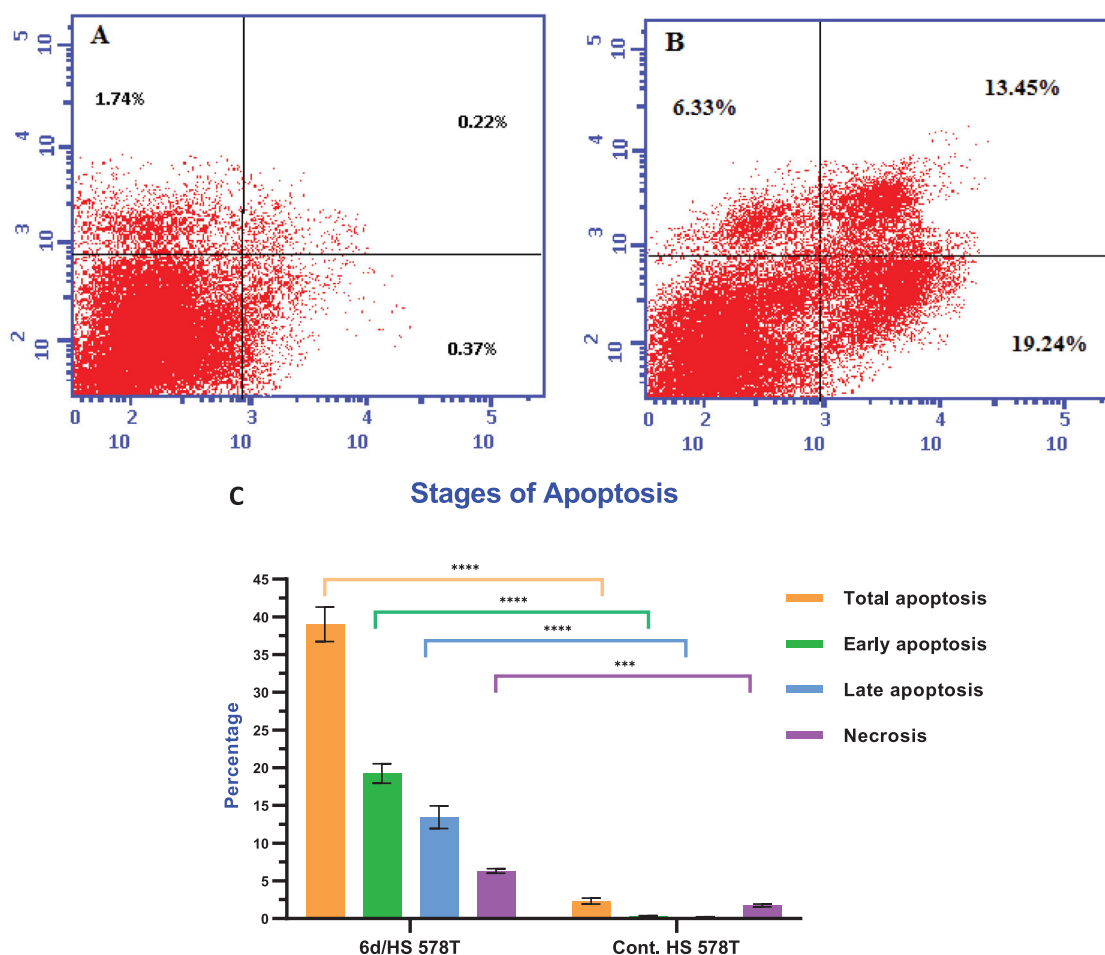


Figure 7. Effect of compound **6d** on Annexin V positive staining percentage in breast cancer HS 578T cells. (A) Control HS 578T; (B) Cells treated with **6d**; (C) Graphical diagram for percentage of apoptotic and necrotic cells in treated cells and untreated control cells. Statistical significance was analysed by two-way ANOVA and Tukey's multiple comparisons test (** $p < 0.001$, **** $p < 0.0001$).

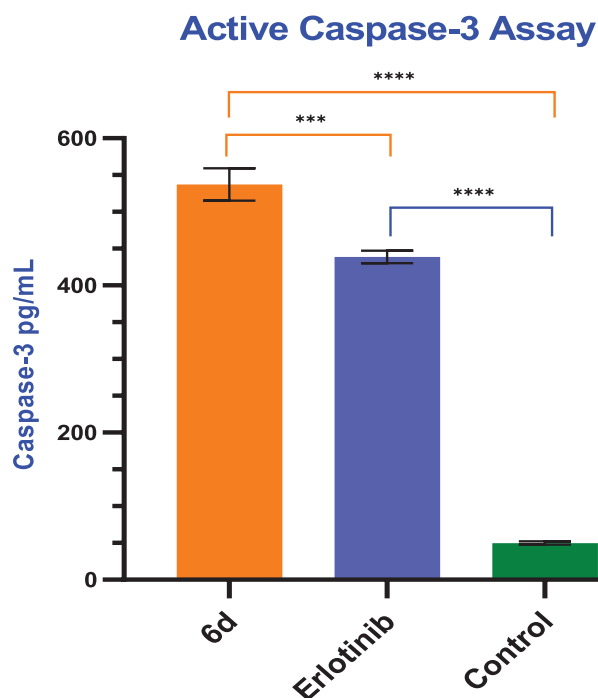


Figure 8. Caspase-3 activity in breast HS 578T cells: Effect of compound **6d** compared to erlotinib. Statistical significance was analysed by one-way ANOVA (** $p < 0.001$, **** $p < 0.0001$).

Table 5. The docking score and Lipinski parameters of compounds **6a**, **6b**, **6d**, **6f** and **6j**.

Compound number	Docking score (PDB):					Interactions
	1M17 (kcal/mol)	HBA (≤ 10)	HBD (≤ 5)	LogP (-4.0 - 5)	PSA (0 - 150) \AA^2	
6a	-8.27	5	1	6.66	83.4	HB (Cys751) Arene-H (Val702)
6b	-8.37	5	1	6.77	83.4	HB (Cys751) Arene-H (Val702)
6d	-8.07	5	1	7.32	83.4	HB (Cys751) Arene-H (Val702) Arene-H (Lys721) Halogen bond (Glu738)
6f	-7.55	6	1	6.67	92.6	HB (Lys721) Arene-H (Val702) Arene-H (Leu694) Halogen bond (Glu738)
6j	-7.98	5	1	5.86	77.4	HB (Cys751) Arene-H (Val702) Arene-H (Lys721) Halogen bond (Glu738)
Erlotinib	-8.68	6	1	2.26	74.7	HB (Cys751) HB (Gln767) HB (Met769) Arene-cation (Lys721)

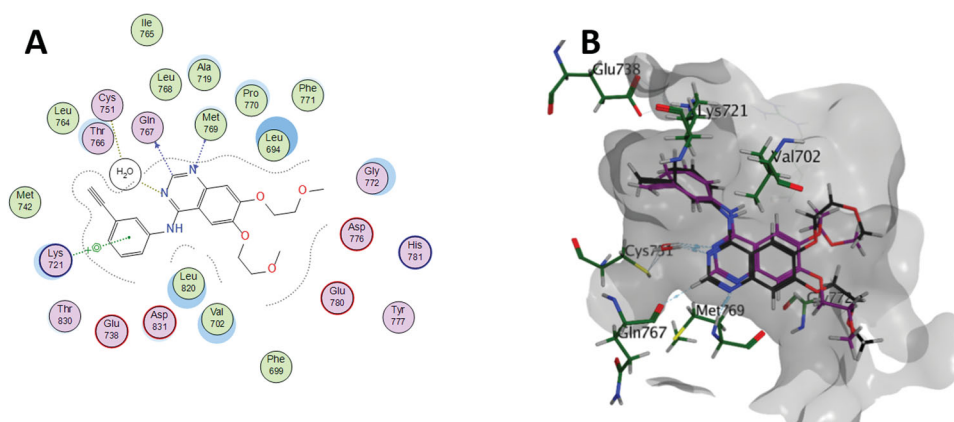


Figure 9. (A) 2D diagram of erlotinib interactions with EGFR binding pocket; (B) 3D overlay of the co-crystallised erlotinib (black) inhibitor and its re-docked pose (magenta) in the binding site of EGFR-TK showing minimum deviation of the docked pose from the co-crystallised one.

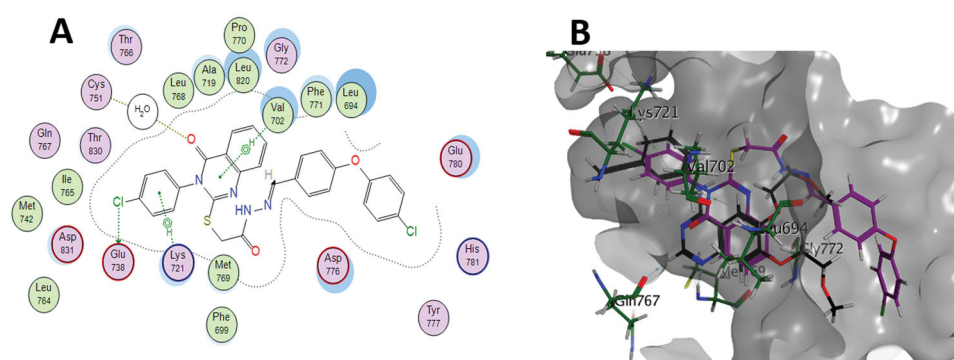


Figure 10. (A) 2D diagram and (B) 3D representation of molecular docking of compound **6d** (magenta) in the binding site of EGFR (PDB: 1M17).

Compound **6f** with $IC_{50} = 0.133 \pm 0.008 \mu M$, showed nearly half the potency of EGFR inhibition compared to compound **6d**. Moreover, compound **6b** was nearly equipotent in EGFR inhibition with compound **6j** with IC_{50} values of 0.487 ± 0.030 and $0.478 \pm 0.029 \mu M$, respectively. Compound **6d**, showed nearly three times the potency of EGFR inhibition compared to compound **6a** with $IC_{50} = 0.202 \pm 0.012 \mu M$. The antiproliferative activity of the compounds correlated with their high ability to inhibit EGFR. These biological results indicate that compound **6d** is a promising antiproliferative agent with EGFR inhibitory activity.

Cell cycle analysis

Most cytotoxic drugs exert their antiproliferative activity by disturbing some checkpoints in the cell cycle. These checkpoints are distinct stages in the cell cycle whose disruption causes growth termination⁴⁶. The cell cycle distribution was measured by DNA flow cytometric analysis, upon incubation of HS578T cells treated with compound **6d** for 24 h at its IC_{50} concentration ($2.17 \mu M$). The effect of compound **6d** on the cell population in different cell phases was recorded and presented in Figure 6. The results were compared to the cell cycle analysis of breast cancer HS 578T cells as untreated control. The proportions of cells in both the G0-G1 phase and the S phase were significantly increased by 1.12-fold. Moreover, significant decrease in the cell population occurred at the G2/M phase with 52%. In comparison to control, the cell population in the pre-G1 phase significantly increased by 16.74-fold. These results showed that, compound **6d** caused induction of cell cycle arrest in breast cancer HS 578T cells at the G1/S phase.

Apoptosis assay

Annexin-V flow cytometry assay is an effective technique to determine apoptosis and for discrimination of programmed apoptosis and non-specific necrosis^{26,47}. Annexin V is a protein with high affinity for phosphatidylserine (PS), a cell membrane component that translocate from the plasma membrane to the surface of the cell during apoptosis. Annexin-V and propidium iodide (PI) dual staining allows for the differentiation of live cells, early/late apoptotic cells, and necrotic cells. Fluorescent Annexin V conjugate can be used to identify PS on the cell surface. PI only enters dead cells and stains DNA⁴⁸. The effect of compound **6d** on cell apoptosis was examined in breast cancer HS 578T cell line using a dual staining assay. The percentage of apoptotic cells increased significantly in early (from 0.37% to 19.24%) and late (from 0.22% to 13.45%) apoptotic phases (Table 4 and Figure 7). Compound **6d** increased total apoptosis significantly by 16.74-fold compared to the control.

Evaluation of caspase-3 activation

Apoptosis is triggered by the activation of caspases, particularly caspase-3, which is an initiator caspase responsible for apoptosis⁴⁹. Therefore, the induction of apoptosis by compound **6d** was examined by the evaluation of caspase-3 activation in breast HS 578T cancer cell line. The effect of erlotinib as well as untreated cell line was used as positive and negative control, respectively. Compound **6d** and erlotinib significantly increased caspase-3 level by 10.75- and 8.78-fold, respectively when compared to negative control Figure 8. These results revealed that

compound **6d** might induce apoptosis *via* a caspase-dependent mechanism.

Molecular docking study

Docking study was carried out for the most potent synthesised compounds into the EGFR protein complexed with erlotinib (PDB: 1M17)⁵⁰ using MOE (2022.09) software⁵¹. The aim of this study was to investigate the interactions between the EGFR-TK and the highly active derivatives, **6a**, **6b**, **6d**, **6f** and **6j**. The study began by redocking the co-crystallised ligand, erlotinib, starting from a two-dimensional structure and using the same protocol for preparation and analysis. The most active derivatives were then docked, and the resulted scores and the binding interactions are included along with the Lipinski parameters in Table 5. Erlotinib fits into the gorge of the active site of EGFR-TK and binds to Cys751 via a water bridge, the N1 atom of the erlotinib accepts a H-bond from the Met769 amide nitrogen. Erlotinib C-2 hydrogen is in close proximity and interacts with Gln767. The anilino ring is coplanar with the quinazoline ring and shows arene-cation interaction with Lys721 (Figure 9). Compounds **6a**, **6b**, **6d**, **6f** and **6j** parameters were aligned with the Lipinski parameters, except for the logP parameter. Generally, compounds **6a**, **6b**, **6d**, **6f** and **6j** were able to overlay as erlotinib with the quinazolinone ring inhabiting the same space of the quinazoline ring of erlotinib. The docking simulation showed that the least active compound **6b** is less binding to the active site with only 2 interactions: [HB (Cys751) and Arene-H (Val702)], while erlotinib has 4 interactions: [HB (Cys751), HB (Gln767), HB (Met769) and Arene-cation (Lys721)]. On the other hand, the docking of the most active compound **6d** (Figure 10) showed a comparable binding profile with the active site as the co-crystallized drug (erlotinib). Compound **6d** forms hydrogen bond with Cys751 via the water bridge and H- π interactions with Val702 which help stabilising the quinazolinone ring conformation. The *p*-chloro phenyl was able to overlay with the anilino ring of erlotinib and also interacts by H- π stacking with Lys721. The chlorine atom forms halogen bond⁵² with the carboxylate group of Glu738 which might be the rationale behind the higher *in vitro* EGFR enzymatic inhibition of **6d** when compared to its dechlorinated congener **6a**. (Docking poses of compounds **6a**, **6b**, **6f** and **6j** are included in supplementary data)

Conclusion

Nineteen quinazolin-4-one derivatives were synthesised to mimic the third generation EGFR TKIs. The antiproliferative activity were assessed for all the prepared compounds. The results showed the significance of the thioacetyl linker for the antiproliferative activity. The compounds showed promising results with **6d** exhibiting high inhibition of EGFR with $IC_{50} = 0.069 \pm 0.004 \mu\text{M}$ which is comparable with the positive control. In addition, **6d** demonstrated an excellent *in vitro* antiproliferative activity with mean growth inhibition of 80.23% and was chosen by the National Cancer Institute (NCI), Maryland, USA for further investigation in which compound **6d** exhibited potent and broad-spectrum antiproliferative activity against most of the tested cancer cell lines, with GI_{50} values in the range of 1.29–5.97 μM . DNA-flow cytometric analysis demonstrated the inhibition of cell proliferation by compound **6d** at G1/S phase. Docking study showed that compound **6d** interacts similarly to erlotinib and highlights the role of

the halogen bond in enhancing the binding to the EGFR binding site for further developments.

Acknowledgements

The authors are thankful to the associates of the National Institutes of Health, USA for performing the anticancer screening. The authors are grateful to Dr. Esam Rashwan, Head of the confirmatory diagnostic unit VACSERA-EGYPT, for carrying out EGFR, caspase-3, cell cycle analysis and apoptosis assays.

Disclosure statement

The authors declare that they do not have conflict of interest. The authors are only responsible for the content and writing of this manuscript.

Funding

The author(s) reported there is no funding associated with the work featured in this article.

References

- Sung H, Ferlay J, Siegel RL, et al. Global cancer statistics 2020: GLOBOCAN estimates of incidence and mortality worldwide for 36 cancers in 185 countries. *CA Cancer J Clin* 2021;71:209–49.
- Lei S, Zheng R, Zhang S, et al. Global patterns of breast cancer incidence and mortality: A population-based cancer registry data analysis from 2000 to 2020. *Cancer Commun* 2021;41:1183–94.
- Lee YT, Tan YJ, Oon CE. Molecular targeted therapy: treating cancer with specificity. *Eur J Pharmacol* 2018;834:188–96.
- Widakowich C, de Azambuja E, Gil T, et al. Molecular targeted therapies in breast cancer: Where are we now? *Int J Biochem Cell Biol* 2007;39:1375–87.
- Maennling AE, Tur MK, Niebert M, et al. Molecular targeting therapy against EGFR family in breast cancer: progress and future potentials. *Cancers (Basel)* 2019;11:1826.
- Habban Akhter M, Sateesh Madhav N, Ahmad J. Epidermal growth factor receptor based active targeting: a paradigm shift towards advance tumor therapy. *Artif Cells, Nanomedicine Biotechnol* 2018;46:1188–98.
- Pellat A, Vaquero J, Fouassier L. Role of ErbB/HER family of receptor tyrosine kinases in cholangiocyte biology. *Hepatology* 2018;67:762–73.
- Mitchell RA, Luwor RB, Burgess AW. Epidermal growth factor receptor: structure-function informing the design of anti-cancer therapeutics. *Exp Cell Res* 2018;371:1–19.
- Kondapaka SB, Fridman R, Reddy KB. Epidermal growth factor and amphiregulin up-regulate matrix metalloproteinase-9 (MMP-9) in human breast cancer cells. *Int J Cancer* 1997;70:722–6.
- Herbst RS. Review of epidermal growth factor receptor biology. *Int J Radiat Oncol Biol Phys* 2004;59:21–6.
- Abdelgawad MA, Bakr RB, Alkhoja OA, Mohamed WR. Design, synthesis and antitumor activity of novel

- pyrazolo[3,4-d]pyrimidine derivatives as EGFR-TK inhibitors. *Bioorg Chem* **2016**;66:88–96.
12. Gaber AA, El-Morsy AM, Sherbiny FF, et al. Pharmacophore-linked pyrazolo[3,4-d]pyrimidines as EGFR-TK inhibitors: synthesis, anticancer evaluation, pharmacokinetics, and in silico mechanistic studies. *Arch Pharm (Weinheim)* **2021**;e2100258.
 13. Le T, Gerber DE. Newer-generation EGFR inhibitors in lung cancer: how are they best used? *Cancers (Basel)* **2019**;11:366.
 14. Mahapatra DK, Das D, Shivhare R. Substituted thiazole linked Murrayanine-Schiff's base derivatives as potential anti-breast cancer candidates: future EGFR kinase inhibitors. *Int J Pharm Sci Drug Res* **2017**;9:139–44.
 15. Zhang H. Three generations of epidermal growth factor receptor tyrosine kinase inhibitors developed to revolutionize the therapy of lung cancer. *Drug Des Devel Ther* **2016**;10:3867–72.
 16. Singh D, Attri BK, Gill RK, Bariwal J. Review on EGFR inhibitors: critical updates. *Mini-Reviews Med Chem* **2016**;16:1134–66.
 17. Ercan D, Choi HG, Yun C-H, et al. EGFR mutations and resistance to irreversible pyrimidine-based EGFR inhibitors. *Clin Cancer Res* **2015**;21:3913–23.
 18. Kwak EL, Sordella R, Bell DW, et al. Irreversible inhibitors of the EGF receptor may circumvent acquired resistance to gefitinib. *Proc Natl Acad Sci U S A* **2005**;102:7665–70.
 19. Miller VA, Hirsh V, Cadranel J, et al. Afatinib versus placebo for patients with advanced, metastatic non-small-cell lung cancer after failure of erlotinib, gefitinib, or both, and one or two lines of chemotherapy (LUX-Lung 1): A phase 2b/3 randomised trial. *Lancet Oncol* **2012**;13:528–38.
 20. Sequist LV, Besse B, Lynch TJ, et al. Neratinib, an irreversible pan-ErbB receptor tyrosine kinase inhibitor: results of a phase II trial in patients with advanced non-small-cell lung cancer. *J Clin Oncol* **2010**;28:3076–83.
 21. Kim Y, Lee S-H, Ahn JS, et al. Efficacy and safety of afatinib for EGFR-mutant non-small cell lung cancer, compared with gefitinib or erlotinib. *Cancer Res Treat* **2019**;51:502–9.
 22. Tan C-S, Kumarakulasinghe NB, Huang Y-Q, et al. Third generation EGFR TKIs: current data and future directions. *Mol Cancer* **2018**;17:1–14.
 23. Hassan RA, Emam SH, Hwang D, et al. Design, synthesis and evaluation of anticancer activity of new pyrazoline derivatives by down-regulation of VEGF: molecular docking and apoptosis inducing activity. *Bioorg Chem* **2022**;118:105487.
 24. El-Dash Y, Elzayat E, Abdou AM, Hassan RA. Novel thienopyrimidine-aminothiazole hybrids: design, synthesis, antimicrobial screening, anticancer activity, effects on cell cycle profile, caspase-3 mediated apoptosis and VEGFR-2 inhibition. *Bioorg Chem* **2021**;114:105137.
 25. Nemr MTM, Sonousi A, Marzouk AA. Design, synthesis and antiproliferative evaluation of new tricyclic fused thiazolopyrimidines targeting topoisomerase II: molecular docking and apoptosis inducing activity. *Bioorg Chem* **2020**;105:104446.
 26. Halim PA, Hassan RA, Mohamed KO, et al. Synthesis and biological evaluation of halogenated phenoxychalcones and their corresponding pyrazolines as cytotoxic agents in human breast cancer. *J Enzyme Inhib Med Chem* **2022**;37:189–201.
 27. Hassan RA, Hamed MIA, Abdou AM, El-dash Y. Novel anti-proliferative agents bearing substituted thieno[2,3-d]pyrimidine scaffold as dual VEGFR-2 and BRAF kinases inhibitors and apoptosis inducers; design, synthesis and molecular docking. *Bioorg Chem* **2022**;125:105861.
 28. Niederst MJ, Hu H, Mulvey HE, et al. The allelic context of the C797S mutation acquired upon treatment with third-generation EGFR inhibitors impacts sensitivity to subsequent treatment strategies. *Clin Cancer Res* **2015**;21:3924–33.
 29. Thress KS, Paweletz CP, Felip E, et al. Acquired EGFR C797S mutation mediates resistance to AZD9291 in non-small cell lung cancer harboring EGFR T790M. *Nat Med* **2015**;21:560–2.
 30. Yan G, Zekarias BL, Li X, et al. Divergent 2-chloroquinazolin-4(3H)-one rearrangement: twisted-cyclic guanidine formation or ring-fused N-acylguanidines via a domino process. *Chem - A Eur J* **2020**;26:2486–92.
 31. Kumari S, Chowdhury J, Sikka M, et al. Identification of potent cholecystokinin-B receptor antagonists: synthesis, molecular modeling and anti-cancer activity against pancreatic cancer cells. *Medchemcomm* **2017**;8:1561–74.
 32. Alanazi AM, Abdel-Aziz AA-M, Shower TZ, et al. Synthesis, antitumor and antimicrobial activity of some new 6-methyl-3-phenyl-4(3H)-quinazolinone analogues: in silico studies. *J Enzyme Inhib Med Chem* **2016**;31:721–35.
 33. El-Azab AS, Abdel-Hamide SG, Sayed-Ahmed MM, et al. Novel 4(3H)-quinazolinone analogs: synthesis and anticonvulsant activity. *Med Chem Res* **2013**;22:2815–27.
 34. Skehan P, Storeng R, Scudiero D, et al. New colorimetric cytotoxicity assay for anticancer-drug screening. *J Natl Cancer Inst* **1990**;82:1107–12.
 35. Boyd MR, Paull KD. Some practical considerations and applications of the national cancer institute in vitro anticancer drug discovery screen. *Drug Dev Res* **1995**;34:91–109.
 36. Shoemaker RH. The NCI60 human tumour cell line anticancer drug screen. *Nat Rev Cancer* **2006**;6:813–23.
 37. Alley MC, Scudiero DA, Monks A, et al. Feasibility of drug screening with panels of human tumor cell lines using a microculture tetrazolium assay. *Cancer Res* **1988**;48:589–601.
 38. Naruse I, Ohmori T, Ao Y, et al. Antitumor activity of the selective epidermal growth factor receptor-tyrosine kinase inhibitor (EGFR-TKI) Iressa® (ZD1839) in an EGFR-expressing multidrug-resistant cell line in vitro and in vivo. *Int J Cancer* **2002**;98:310–5.
 39. Tolba MF, Esmat A, Al-Abd AM, et al. Caffeic acid phenethyl ester synergistically enhances docetaxel and paclitaxel cytotoxicity in prostate cancer cells. *IUBMB Life* **2013**;65:716–29.
 40. Rieger AM, Nelson KL, Konowalchuk JD, Barreda DR. Modified annexin V/propidium iodide apoptosis assay for accurate assessment of cell death. *J Vis Exp* **2011**;50:e2597.
 41. Maher M, Kassab AE, Zaher AF, Mahmoud Z. Novel pyrazolo[3,4-d]pyrimidines: design, synthesis, anticancer activity, dual EGFR/ErbB2 receptor tyrosine kinases inhibitory activity, effects on cell cycle profile and caspase-3-mediated apoptosis. *J Enzyme Inhib Med Chem* **2019**;34:532–46.
 42. Shawali AS, Hassaneen HM, Shurrab NK. A new convenient synthesis of 2,4-disubstituted-1,2,4-triazolo[1,5-a]quinazolin-5(4H)-ones. *J Heterocycl Chem* **2008**;45:1825–9.
 43. Tavakol H, Farrokhpour H. DFT and MP2 study of low barrier proton transfer in hydrazide schiff base tautomers via water bridges and in the gas. *J Mol Model* **2013**;19:3471–9.
 44. Sakr A, Rezaq S, Ibrahim SM, et al. Design and synthesis of novel quinazolinones conjugated ibuprofen indole acetamide or thioacetohydrazide as selective COX 2 inhibitors:

- anti-inflammatory, analgesic and anticancer activities. *J Enzyme Inhib Med Chem* [2021](#);36:1810–28.
45. El-Sayed S, Metwally K, El-Shanawani AA, Abdel-Aziz LM, et al. Synthesis and anticancer activity of novel quinazolinone-based rhodanines. *Chem Cent J* [2017](#);11:102.
46. Matson JP, Cook JG. Cell cycle proliferation decisions: the impact of single cell analyses. *FEBS J* [2017](#);284:362–75.
47. Gorczyca W. Cytometric analyses to distinguish death processes. *Endocr Relat Cancer* [1999](#);6:17–9.
48. Utsuro M. Neutron spin interference visibility in tunneling transmission through magnetic resonators. *Phys B Condens Matter* [2005](#);358:232–46.
49. Gong L, Tang Y, An R, et al. RTN1-C mediates cerebral ischemia/reperfusion injury via ER stress and mitochondria-associated apoptosis pathways. *Cell Death Dis* [2017](#);8:e3080.
50. Stamos J, Sliwkowski MX, Eigenbrot C. Structure of the epidermal growth factor receptor kinase domain alone and in complex with a 4-anilinoquinazoline inhibitor. *J Biol Chem* [2002](#);277:46265–72.
51. Molecular Operating Environment (MOE), 2020.09 Chemical Computing Group ULC, 1010 Sherbooke St. West, Suite #910, Montreal, QC, Canada, H3A 2R7. [2022](#).
52. Cavallo G, Metrangolo P, Milani R, et al. The halogen bond. *Chem Rev* [2016](#);116:2478–601.